Even exciton series in Cu_2O

Frank Schweiner, Jörg Main, and Günter Wunner
Institut für Theoretische Physik 1, Universität Stuttgart, 70550 Stuttgart, Germany

Christoph Uihlein
Experimentelle Physik 2, Technische Universität Dortmund, 44221 Dortmund, Germany
(Received 8 February 2017; revised manuscript received 28 March 2017; published 1 May 2017)

Recent investigations of excitonic absorption spectra in cuprous oxide (Cu_2O) have shown that it is indispensable to account for the complex valence-band structure in the theory of excitons. In Cu_2O, parity is a good quantum number and thus the exciton spectrum falls into two parts: the dipole-active exciton states of negative parity and odd angular momentum, which can be observed in one-photon absorption (Γ_4^- symmetry), and the exciton states of positive parity and even angular momentum, which can be observed in two-photon absorption (Γ_5^+ symmetry). The unexpected observation of D excitons in two-photon absorption has given first evidence that the dispersion properties of the Γ_5^+ orbital valence band are giving rise to a coupling of the yellow and green exciton series. However, a first theoretical treatment by Uihlein *et al.* [Phys. Rev. B **23**, 2731 (1981)] was based on a simplified spherical model. The observation of F excitons in one-photon absorption is a further proof of a coupling between yellow and green exciton states. Detailed investigations on the fine structure splitting of the F exciton by F. Schweiner *et al.* [Phys. Rev. B **93**, 195203 (2016)] have proved the importance of a more realistic theoretical treatment including terms with cubic symmetry. In this paper we show that the even and odd parity exciton system can be consistently described within the same theoretical approach. However, the Hamiltonian of the even parity system needs, in comparison to the odd exciton case, modifications to account for the very small radius of the yellow and green $1S$ exciton. In the presented treatment, we take special care of the central-cell corrections, which comprise a reduced screening of the Coulomb potential at distances comparable to the polaron radius, the exchange interaction being responsible for the exciton splitting into ortho and para states, and the inclusion of terms in the fourth power of p in the kinetic energy being consistent with O_h symmetry. Since the yellow $1S$ exciton state is coupled to all other states of positive parity, we show how the central-cell corrections affect the whole even exciton series. The close resonance of the $1S$ green exciton with states of the yellow exciton series has a strong impact on the energies and oscillator strengths of all implied states. The consistency between theory and experiment with respect to energies and oscillator strengths for the even and odd exciton system in Cu_2O is a convincing proof for the validity of the applied theory.

DOI: 10.1103/PhysRevB.95.195201

I. INTRODUCTION

Excitons are the quanta of fundamental optical excitations in both insulators and semiconductors in the visible and ultraviolet spectrum of light. The Coulomb interaction between electron and hole leads to a hydrogenlike series of excitonic states [1]. Cuprous oxide (Cu_2O) is a prime example where one can even identify four different excitonic series (yellow, green, blue, and violet) being related to the two topmost valence bands and the two lowest conduction bands [2]. Recently, the yellow series could be followed up to a spectacular high principal quantum number of $n = 25$ [2]. This outstanding experiment has launched the new field of research of giant Rydberg excitons and led to a variety of new theoretical and experimental investigations on the topic of excitons in Cu_2O [3–16].

Cu_2O has octahedral symmetry O_h so that the symmetry of the bands can be assigned by the irreducible representations $\Gamma_i^{\pm}$ of O_h. The yellow and green exciton series share the same threefold degenerate Γ_5^+ orbital valence-band state. This state splits due to spin-orbit interaction into an upper twofold degenerate Γ_7^+ valence band (yellow series) and a lower fourfold degenerate Γ_8^+ valence band (green series). The band structure of both bands is essentially determined by the anisotropic dispersion properties of the orbital state. The threefold degeneracy of the orbital state is lifted as soon as a nonzero k vector gets involved, with new eigenvectors depending on the orientation of $\boldsymbol{k}$. A consequence of the splitting of the orbital state is a partial quenching of the spin-orbit interaction. This $\boldsymbol{k}$-dependent quenching is not only responsible for a remarkable nonparabolicity of the two top valence bands but leads likewise to a $\boldsymbol{k}$-dependent mixing of the Γ_7^+ and Γ_8^+ Bloch states and can thus cause a mixing of the yellow and green exciton series. A mixing of both series is favored by the large Rydberg energy of approximately 100 meV, a corresponding large exciton extension in k space and the small spin-orbit splitting of only 130 meV.

A Hamiltonian that is able to cope with a coupled system of yellow and green excitons must take explicit care of the dispersion properties of the orbital valence-band state and has to include the spin-orbit interaction. Such a kind of Hamiltonian was first introduced by Uihlein *et al.* [17] for explaining the unexpected fine structure splitting observed in the two-photon absorption spectrum of Cu_2O. They used a simplified spherical dispersion model for the Γ_5^+ orbital valence band with an identical splitting into longitudinal and transverse states independent of the orientation of $\boldsymbol{k}$. This simplification had the appealing advantage that the total angular momentum remains a good quantum number

so that the exciton problem could be reduced to calculate the eigenvalues of a system of coupled radial wave functions. A problem in their paper is the incorrect notation of the $1S$ green and $2S$ yellow excitons states. Both notations need to be exchanged to be consistent with their calculations. Although the spherical model can explain many details of the experimental findings, one has to be aware of its limitations. A more realistic Hamiltonian being compliant with the real band structure by including terms of cubic symmetry has already proved its validity by explaining the puzzling fine structure of the odd parity states in Cu_2O [10]. The intention of this paper is to show that the same kind of Hamiltonian can likewise describe the fine splitting of the even parity excitons.

However, when comparing the even parity and odd parity exciton systems, it is obvious that the even exciton system is a much more challenging problem. One reason for this is the close resonance of the green $1S$ exciton with the even parity states of the yellow series with principal quantum number $n \geqslant 2$. This requires a very careful calculation of the binding energy of the green $1S$ exciton. Furthermore, the binding energy of the yellow $1S$ exciton is much larger than expected from a simple hydrogenlike series, inter alia, due to a less effective screening of the Coulomb potential at distances comparable to the polaron radius. Moreover, a breakdown of the electronic screening is expected at even much shorter distances, but a proper treatment is exceeding the limits of the continuum approximation. Hence we introduce in this paper a δ-functionlike central cell correction term that should account for all kinds of short range perturbations affecting the immediate neighborhood of the central cell. The magnitude of this term is treated as a free parameter that can be adjusted to the experimental findings. It is important to note that a change of this parameter leads to a significant shift of the green $1S$ exciton with respect to the higher-order states of the yellow series and has therefore a high impact on the energies and the compositions of the resulting coupled exciton states. Taking this in mind it is fundamental that one can likewise achieve a match to the relative oscillator strengths of the involved states.

Dealing with the even parity system of Cu_2O is also confronting us with the problem of a proper treatment of the $1S$ exciton with respect to its very small radius since a small exciton radius means a large extension of the exciton in k space. The challenge is therefore to meet the band structure of the valence band in a much larger vicinity of the Γ point. For coping with this situation, we include in the kinetic energy of the hole all terms in the fourth power of p being compliant with the octahedral symmetry of Cu_2O. The parameters of these terms are carefully adjusted to get a best fit to the band structure in the part of the k space being relevant for the $1S$ exciton.

Despite of all these modifications, it is important to note that the Hamiltonian is essentially the same as the one being applied to the odd exciton system [10]. The fundamental modifications presented in this paper are irrelevant for the odd parity system because of their δ-functionlike nature or their specific form affecting only exciton states with a small radius. Hence we present a consistent theoretical model for the complete exciton spectrum of Cu_2O.

Comparing our results to experimental data, we can prove very good agreement as regards not only the energies but also the oscillator strengths since our method of solving the Schrödinger equation allows us also to calculate relative oscillator strengths for one-photon and two-photon absorption. This agreement between theory and experiment is important not only for the investigation of exciton spectra in electric or combined electric and magnetic fields. A correct theoretical description of excitons is indispensable if Rydberg excitons will be used in the future in quantum information technology, or used to attain a deeper understanding of quasi-particle interactions in semiconductors [2,16]. Furthermore, this agreement is a prerequisite for a future search for exceptional points in the exciton spectrum [8].

The paper is organized as follows: having presented the Hamiltonian of excitons in Cu_2O when considering the complete valence-band structure in Sec. II, we discuss all corrections to this Hamiltonian due to the small radius of the $1S$ exciton in Sec. III. In Sec. IV, we show how to solve the Schrödinger equation using a complete basis and how to calculate relative oscillator strengths for one-photon and two-photon absorption. In Sec. V, we discuss the complete yellow and green exciton spectrum of Cu_2O paying attention to the exciton states with a small principal quantum number and especially to the green $1S$ exciton state. Finally, we give a short summary and outlook in Sec. VI.

II. HAMILTONIAN

In this section, we present the Hamiltonian of excitons in Cu_2O, which accounts for the complete valence-band structure of this semiconductor. This Hamiltonian describes the exciton states of odd parity with a principal quantum number $n \geqslant 3$ very well [10,14]. However, for the exciton states of even parity and for the $2P$ exciton corrections to this Hamiltonian are needed, which will be described in Sec. III.

The lowest Γ_6^+ conduction band in Cu_2O is almost parabolic in the vicinity of the Γ point and the kinetic energy can be described by the simple expression

$$H_e(\boldsymbol{p}_e) = \frac{\boldsymbol{p}_e^2}{2m_e}, \tag{1}$$

with the effective electron mass m_e. Since Cu_2O has cubic symmetry, we use the irreducible representations $\Gamma_i^{\pm}$ of the cubic group O_h to assign the symmetry of the bands.

Due to interband interactions and nonparabolicities of the three uppermost valence bands in Cu_2O, the kinetic energy of the hole is given by the more complex expression [9,10,14],

$$\begin{aligned} H_h(\boldsymbol{p}_h) = H_{so} + (1/2\hbar^2 m_0)\big\{&\hbar^2(\gamma_1 + 4\gamma_2)\boldsymbol{p}_h^2 \\ &+ 2(\eta_1 + 2\eta_2)\boldsymbol{p}_h^2(\boldsymbol{I}\cdot\boldsymbol{S}_h) \\ &- 6\gamma_2\big(p_{h1}^2\boldsymbol{I}_1^2 + \text{c.p.}\big) - 12\eta_2\big(p_{h1}^2\boldsymbol{I}_1\boldsymbol{S}_{h1} + \text{c.p.}\big) \\ &- 12\gamma_3(\{p_{h1},p_{h2}\}\{\boldsymbol{I}_1,\boldsymbol{I}_2\} + \text{c.p.}) \\ &- 12\eta_3(\{p_{h1},p_{h2}\}(\boldsymbol{I}_1\boldsymbol{S}_{h2} + \boldsymbol{I}_2\boldsymbol{S}_{h1}) + \text{c.p.})\big\} \end{aligned} \tag{2}$$

with $\{a,b\} = \frac{1}{2}(ab + ba)$, the free electron mass m_0, and c.p. denoting cyclic permutation. The quasispin $I = 1$ describes

the threefold degenerate valence band and is a convenient abstraction to denote the three orbital Bloch functions xy, yz, and zx [18]. The parameters γ_i, which are called the first three Luttinger parameters, and the parameters η_i describe the behavior and the anisotropic effective mass of the hole in the vicinity of the Γ point. The spin-orbit coupling, which enters Eq. (2), is given by

$$H_{\mathrm{so}} = \frac{2}{3}\Delta\left(1 + \frac{1}{\hbar^2}\boldsymbol{I}\cdot\boldsymbol{S}_{\mathrm{h}}\right). \tag{3}$$

In a first approximation, the interaction between the electron and the hole is described by a screened Coulomb potential

$$V(\boldsymbol{r}_e - \boldsymbol{r}_h) = -\frac{e^2}{4\pi\varepsilon_0\varepsilon_{\mathrm{s1}}}\frac{1}{|\boldsymbol{r}_e - \boldsymbol{r}_h|} \tag{4}$$

with the dielectric constant $\varepsilon_{\mathrm{s1}} = 7.5$. For small relative distances $r = |\boldsymbol{r}| = |\boldsymbol{r}_e - \boldsymbol{r}_h|$ corrections to this potential and to the kinetic energies $H_{\mathrm{e}}(\boldsymbol{p}_{\mathrm{e}})$ and $H_{\mathrm{h}}(\boldsymbol{p}_{\mathrm{h}})$ are needed, which will be described in Sec. III and which will be denoted here by V_{CCC}.

After introducing relative and center of mass coordinates [19] and setting the position and momentum of the center of mass to zero, the complete Hamiltonian of the relative motion finally reads [17,20]

$$H = E_{\mathrm{g}} + V(\boldsymbol{r}) + H_{\mathrm{e}}(\boldsymbol{p}) + H_{\mathrm{h}}(\boldsymbol{p}) + V_{\mathrm{CCC}} \tag{5}$$

with the energy E_{g} of the band gap.

Note that by setting the total momentum to zero, we neglect polariton effects, even though in experiments the polaritonic part is always present. However, when considering the experimental results of Refs. [21–23], the polariton effect on the $1S$ exciton is on the order of tens of μeV and, hence, much smaller than the energy shifts considered here. Furthermore, in Ref. [24], criteria for the experimental observability of polariton effects are given. Inserting the material parameters of Cu_2O and the experimental linewidths of the exciton states observed in Refs. [2,3], it can be shown that polariton effects are not observable for the exciton states of $n \geqslant 2$. We will discuss this in greater detail in a future work.

III. CENTRAL-CELL CORRECTIONS

Due to its small radius, the $1S$ exciton in Cu_2O is an exciton intermediate between a Frenkel and a Wannier exciton [1]. Hence appropriate corrections are needed to describe this exciton state correctly. The corrections, which allow for the best possible description of the exciton problem within the continuum approximation of the solid, are called central-cell corrections and have first been treated by Uihlein *et al.* [17,25] and Kavoulakis *et al.* [26] for Cu_2O. While Uihlein *et al.* [17] accounted for these corrections only in a simplified way by using a semiempirical contact potential $V = -V_0\delta(\boldsymbol{r})$, the treatment of Kavoulakis *et al.* [26] did non account for the band structure and the effect of the central-cell corrections was discussed only on the $1S$ state and only using perturbation theory. By considering the complete valence-band structure of Cu_2O in combination with a nonperturbative treatment of the central-cell corrections, we present a more accurate treatment of the whole yellow exciton series in Cu_2O. Corrections beyond the frame of the continuum approximation will not be treated here. However, these corrections may describe remaining small deviations between experimental and theoretical results.

The central-cell corrections as discussed in Ref. [26] comprise three effects, which are (i) the appearance of terms of higher order in the momentum $\boldsymbol{p}$ in the kinetic energies of electron and hole, (ii) the momentum and frequency dependence of the dielectric function ε, and (iii) the appearance of an exchange interaction, which depends on the momentum of the center of mass.

A. Band structure of Cu_2O

Since the radius of the yellow $1S$ exciton is small, the extension of its wave function in momentum space is accordingly large. Hence we have to consider terms of the fourth power of $\boldsymbol{p}$ in the kinetic energy of the electron and the hole. The inclusion of p^4 terms in Eqs. (1) and (2) leads to an extended and modified Hamiltonian in the sense of Altarelli, Baldereschi, and Lipari [20,27–30] or Suzuki and Hensel [31].

The extended Hamiltonian must be compatible with the symmetry O_{h} of the crystal and transform according to the irreducible representation Γ_1^+. All the terms of the fourth power of $\boldsymbol{p}$ span a fifteen-dimensional space with the basis functions

$$p_i^4, \quad p_i^3 p_j, \quad p_i^2 p_j^2, \quad p_i p_j p_k^2 \tag{6}$$

with $i,j,k \in \{1,2,3\}$ and $i \neq j \neq k \neq i$. Including the quasispin I and using group theory, one can find six linear combinations of p^4 terms, which transform according to Γ_1^+ [32] (see Appendix A). Using the results of Appendix A, we can write the kinetic energy of the electron and the hole as

$$H_{\mathrm{e}}(\boldsymbol{p}_{\mathrm{e}}) = \frac{1}{2\hbar^2 m_{\mathrm{e}}}\left\{\left(\hbar^2 + \lambda_1 a^2 \boldsymbol{p}_{\mathrm{e}}^2\right)\boldsymbol{p}_{\mathrm{e}}^2 + \lambda_2 a^2\left[p_{\mathrm{e1}}^2 p_{\mathrm{e2}}^2 + \mathrm{c.p.}\right]\right\} \tag{7}$$

and

$$\begin{aligned} H_{\mathrm{h}}(\boldsymbol{p}_{\mathrm{h}}) = H_{\mathrm{so}} + \frac{1}{2\hbar^4 m_0}\Big\{&(\gamma_1 + 4\gamma_2)\hbar^2\left(\hbar^2 + \xi_1 a^2 \boldsymbol{p}_{\mathrm{h}}^2\right)\boldsymbol{p}_{\mathrm{h}}^2 + \xi_2 a^2\hbar^2\left[p_{\mathrm{h1}}^2 p_{\mathrm{h2}}^2 + \mathrm{c.p.}\right] \\ &- 6\gamma_2\left(\hbar^2 + \xi_3 a^2 \boldsymbol{p}_{\mathrm{h}}^2\right)\left[p_{\mathrm{h1}}^2 \boldsymbol{I}_1^2 + \mathrm{c.p.}\right] - 12\gamma_3\left(\hbar^2 + \xi_4 a^2 \boldsymbol{p}_{\mathrm{h}}^2\right)[p_{\mathrm{h1}} p_{\mathrm{h2}}\{\boldsymbol{I}_1, \boldsymbol{I}_2\} + \mathrm{c.p.}] \\ &+ 2(\eta_1 + 2\eta_2)\hbar^2\left[\boldsymbol{p}_{\mathrm{h}}^2\, \boldsymbol{I}\cdot\boldsymbol{S}_{\mathrm{h}}\right] - 12\eta_2\hbar^2\left[p_{\mathrm{h1}}^2 \boldsymbol{I}_1 \boldsymbol{S}_{\mathrm{h1}} + \mathrm{c.p.}\right] - 12\eta_3\hbar^2[p_{\mathrm{h1}} p_{\mathrm{h2}}(\boldsymbol{I}_1 \boldsymbol{S}_{\mathrm{h2}} + \boldsymbol{I}_2 \boldsymbol{S}_{\mathrm{h1}}) + \mathrm{c.p.}] \\ &- 6\xi_5 a^2\left[\left(p_{\mathrm{h1}}^4 + 6p_{\mathrm{h2}}^2 p_{\mathrm{h3}}^2\right)\boldsymbol{I}_1^2 + \mathrm{c.p.}\right] - 12\xi_6 a^2\left[\left(p_{\mathrm{h1}}^2 + p_{\mathrm{h2}}^2 - 6p_{\mathrm{h3}}^2\right)p_{\mathrm{h1}} p_{\mathrm{h2}}\{\boldsymbol{I}_1, \boldsymbol{I}_2\} + \mathrm{c.p.}\right]\Big\} \end{aligned} \tag{8}$$

TABLE I. Material parameters used in the calculations. Instead of the band-gap energy $E_g = 2.17208$ eV of Ref. [2] a slightly smaller value is used to obtain a better agreement with experimental values in Sec. V.

band-gap energy	$E_g = 2.17202$ eV	
electron mass	$m_e = 0.99\,m_0$	[68]
spin-orbit coupling	$\Delta = 0.131$ eV	[9]
valence-band parameters	$\gamma_1 = 1.76$	[9,10]
	$\gamma_2 = 0.7532$	[9,10]
	$\gamma_3 = -0.3668$	[9,10]
	$\eta_1 = -0.020$	[9,10]
	$\eta_2 = -0.0037$	[9,10]
	$\eta_3 = -0.0337$	[9,10]
lattice constant	$a = 0.42696$ nm	[69]
dielectric constants	$\varepsilon_{s1} = 7.5$	[43]
	$\varepsilon_{b1} = \varepsilon_{s2} = 7.11$	[43]
	$\varepsilon_{b2} = 6.46$	[43]
energy of Γ_4^--LO phonons	$\hbar\omega_{LO1} = 18.7$ meV	[26]
	$\hbar\omega_{LO2} = 87$ meV	[26]

with the lattice constant a and the unknown parameters λ_i and ξ_i. Note that the values of parameters η_i are smaller than the Luttinger parameters γ_i (see Table I). Hence we expect the terms of the form $p^4 I S_h$ to be negligibly small.

After replacing $H_e(\boldsymbol{p}_e) \to H_e(\hbar\boldsymbol{k})$ and $H_h(\boldsymbol{p}_h) \to -H_h(\hbar\boldsymbol{k})$, we can determine the eigenvalues of these Hamiltonians and fit them as in Ref. [9] for $|\boldsymbol{k}| < \pi/a$ to the band structure of Cu_2O obtained via spin density functional theory calculations [33].

To obtain a reliable result, we perform a least-squares fit with a weighting function. Even though the exciton ground state will show deviations from a pure hydrogenlike $1S$ state, we expect that the radial probability density can be described qualitatively by that function. Hence we use the modulus squared of the Fourier transform $\Phi_{1S}(\boldsymbol{k}) = \mathcal{F}(\Psi_{1S})(\boldsymbol{k})$ of the hydrogenlike function

$$\Psi_{1S}(\boldsymbol{r}) = \frac{1}{\sqrt{\pi\left(a_{\mathrm{exc}}^{(1S)}\right)^3}} e^{-r/a_{\mathrm{exc}}^{(1S)}} \tag{9}$$

as the weighting function for the fit. It reads [34]

$$|\Phi_{1S}(\boldsymbol{k})|^2 \sim \left| \frac{1}{\sqrt{(2\pi)^3}} \int \mathrm{d}\boldsymbol{r}\ \Psi_{1S}(\boldsymbol{r}) e^{-i\boldsymbol{k}\boldsymbol{r}} \right|^2$$

$$= \frac{8\left(a_{\mathrm{exc}}^{(1S)}\right)^3}{\pi^2\left(1 + k^2\left(a_{\mathrm{exc}}^{(1S)}\right)^2\right)^4} \tag{10}$$

with the radius $a_{\mathrm{exc}}^{(1S)}$ of the $1S$ exciton state. Although we do not *a priori* know the true value of $a_{\mathrm{exc}}^{(1S)}$, the experimental value of the binding energy of the $1S$ state [1,17] as well as the calculations of Ref. [26] indicate that it is on the order of one or two times the lattice constant $a = 0.427$ nm [35–37]. For the fit to the band structure we assume a small value of $a_{\mathrm{exc}}^{(1S)} = a$ as a lower limit in the sense of a safe estimate since then the extension of the exciton wave function in Fourier space is larger. In doing so, we will now show that even if the radius of the $1S$ exciton were smaller or equal to the lattice constant a, there would not be contributions of the p^4 terms of the band structure.

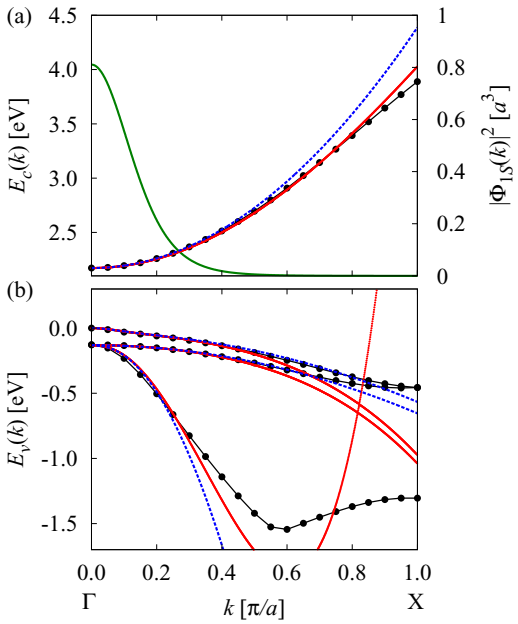

FIG. 1. Fits to the band structure obtained via spin density functional theory calculations [33] (black linespoints) for (a) conduction and (b) valence bands of Cu_2O for the [100] direction using the expressions (7) and (8) (red lines). The green solid line shows the function $|\Phi_{1S}(\boldsymbol{k})|^2$ for $a_{\mathrm{exc}}^{(1S)} = a$ in units of a^3. One can see that the differences between the fit using quartic terms and the fit of Ref. [9] (blue dashed lines) neglecting these terms are small in the range of extension of $|\Phi_{1S}(\boldsymbol{k})|^2$. Note that $|\Phi_{1S}(\boldsymbol{k})|^2$ is not shown in the lower panel for reasons of clarity.

The results of the fit are depicted as red solid lines in Figs. 1–3. For a comparison, we also show the fit neglecting the quartic terms in the momenta (blue dashed lines) [9]. The values of the fit parameters are

$$\begin{aligned} &\lambda_1 = -1.109 \times 10^{-2}, \quad \lambda_2 = -2.052 \times 10^{-2}, \\ &\xi_1 = -1.389 \times 10^{-1}, \quad \xi_4 = -1.518 \times 10^{-1}, \\ &\xi_2 = 2.353 \times 10^{-3}, \quad \xi_5 = 9.692 \times 10^{-4}, \\ &\xi_3 = -1.523 \times 10^{-1}, \quad \xi_6 = -8.385 \times 10^{-4}. \end{aligned} \tag{11}$$

As can be seen, e.g., from Fig. 2, the fit including the quartic terms is only slightly better than the fit with the quadratic terms for small k. A clear difference between the fits can be seen only for large values of k as regards the valence bands: since some of the prefactors of the quartic terms are positive, the energy of the valence bands in the fitted model increases for larger values of k.

Considering the minor differences between the fits for small k and the small extension of the $1S$ exciton function in k space even for $a_{\mathrm{exc}}^{(1S)} = a$ (see, e.g., Fig. 1), the quartic terms will hardly affect this exciton state and can be neglected. These arguments still hold if, e.g., $a_{\mathrm{exc}}^{(1S)} = 0.2a$ is assumed.

In the work of Ref. [26], the introduction of p^4 terms seemed necessary to explain the experimentally observed large mass of the $1S$ exciton. However, the experimental observations are already well described by quadratic terms in

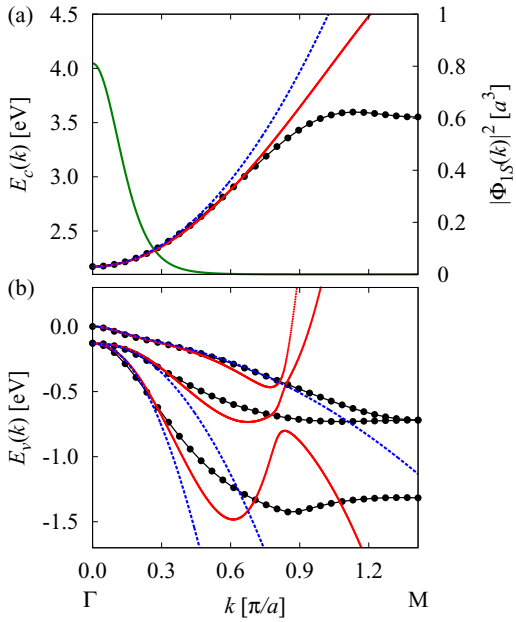

FIG. 2. Same as Fig. 1 for the [110] direction.

p when considering the complete valence-band structure [10]. As we already stated in Ref. [13], a simple restriction to the Γ_7^+ band neglecting the Γ_8^+ band and considering the nonparabolicity of the Γ_7^+ band via p^4 terms as has been done in Ref. [26] does not treat the problem correctly.

B. Dielectric constant

In the case of the $1S$ exciton in Cu_2O, the relative motion of the electron and the hole is sufficiently fast that phonons cannot follow it and corrections on the dielectric constant need to be considered. In general, the electron and the hole

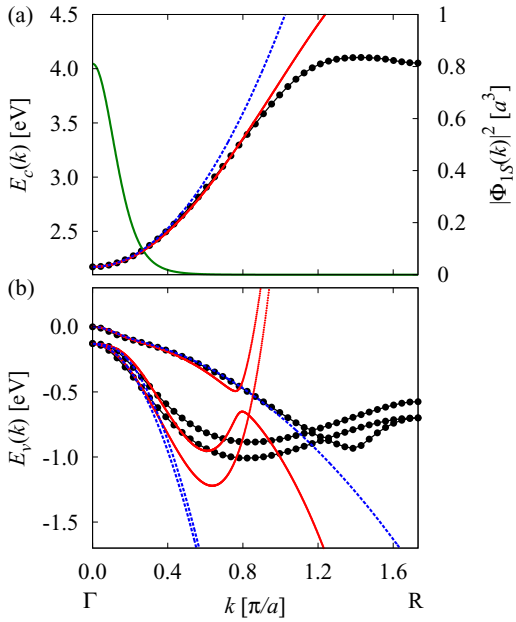

FIG. 3. Same as Fig. 1 for the [111] direction.

are coupled to longitudinal optical phonons via the Fröhlich interaction [38,39] and to longitudinal acoustic phonons via the deformation potential coupling [39,40]. While in the case of optical phonons, the ions of the solid are displaced in antiphase and thus create a dipole moment in the unit cell of a polar crystal, the ions are displaced in phase in the case of acoustic phonons and no dipole moment is created. Hence one expects that the interaction between electron or hole and optical phonons is much larger than the interaction with acoustic phonons in polar crystals [41,42].

If the frequency of the relative motion of electron and hole is high enough so that the ions of the solid cannot follow it, the Coulomb interaction between electron and hole is screened by the high-frequency or background dielectric constant ε_b [1,43]. This dielectric constant describes the electronic polarization, which can follow the motion of electron and hole very quickly [44].

For lower frequencies of the relative motion, the contribution of the phonons to the screening becomes important and the dielectric function ε becomes frequency dependent. In many semiconductors, the frequency of the relative motion in exciton states with a principal quantum number of $n \geqslant 2$ is so small that the low-frequency or static dielectric constant ε_s can be used [42], which involves the electronic polarization *and* the displacement of the ions [44]. Note that we use the notation ε_b, ε_s instead of ε_∞, ε_0 to avoid the risk of confusion with the electric permittivity ε_0 [42,44].

The transition from $-e^2/4\pi\varepsilon\varepsilon_s r$ to $-e^2/4\pi\varepsilon\varepsilon_b r$, which takes place when the frequency of the electron or the hole is of the same size as the frequency of the phonon [44], had been investigated in detail by Haken in Refs. [41,44–48]. He considered at first the interaction between electron or hole and the phonons and then constructed the exciton from the resulting particles with polarization clouds, i.e., the polarons. The change of the Coulomb interaction between both particles was then explained in terms of an exchange of phonons, i.e., of virtual quanta of the polarization field [44].

The final result for the interaction in the transition region between $-e^2/4\pi\varepsilon_0\varepsilon_s r$ and $-e^2/4\pi\varepsilon_0\varepsilon_b r$ was the so-called Haken potential [1,34,42,46–48],

$$V(r) = -\frac{e^2}{4\pi\varepsilon_0 r}\left[\frac{1}{\varepsilon_s} + \frac{1}{2\varepsilon^*}(e^{-r/\rho_h} + e^{-r/\rho_e})\right]. \quad (12)$$

Here, ρ_e and ρ_h denote the polaron radii

$$\rho_{e/h} = \sqrt{\frac{\hbar}{2m^*_{e/h}\omega_{LO}}} \quad (13)$$

with the frequency ω_{LO} of the optical phonon and ε^* given by

$$\frac{1}{\varepsilon^*} = \frac{1}{\varepsilon_b} - \frac{1}{\varepsilon_s}. \quad (14)$$

Note that in the result of Haken the polaron masses m_i^* instead of the bare electron and hole masses have to be used in the polaron radii and the kinetic energies [41,49]. Furthermore, the lattice relaxation due to the interaction of excitons and phonons decreases the band-gap energy for electrons and holes. However, since the value of E_g for Cu_2O has been determined in Ref. [2] from the experimental exciton spectrum, the polaron effect is already accounted for in the band-gap energy [42].

Note that the above results were derived in the simple band model and by assuming only one optical phonon branch contributing to the Fröhlich interaction. To the best of our knowledge, there is no model accounting for more than one optical phonon branch [26,44,49], which complicates the correct treatment of Cu_2O, where two LO phonons contribute to the Fröhlich interaction. Even though there are theories for polarons in the degenerate band case [50–52], we will use only the leading, spherically symmetric terms, in which only the isotropic effective mass of the hole or only the Luttinger parameter γ_1 enters. Of course, there are further terms of cubic symmetry, which also depend on the other Luttinger parameters. However, since already γ_1 is at least by a factor of 2 larger than the other Luttinger parameters, we expect the further terms in the Haken potentials to be smaller than the leading term used here. Since the effect of the Haken potential on the exciton spectrum is not crucial, as will be seen from Fig. 6, the neglect of further terms in the polaron potentials will then be *a posteriori* justified.

Furthermore, the Haken potential (12) cannot describe the non-Coulombic electron-hole interaction for very small values of r, which is due to the finite size of electron and hole [1]. The conditions of validity of the potential (12) have, e.g., been discussed by Haken in Ref. [44].

When treating the Haken potential numerically for different polar crystals, the experimental and theoretical binding energies of the exciton states sometimes do not agree, for which reason corrections, sometimes phenomenologically, to the Haken potential have been introduced [53–56] leading to clearly better results. One of these refined formulas is the potential proposed by Pollmann and Büttner [49,56]

$$V(r) = -\frac{e^2}{4\pi\varepsilon_0 r} \times \left[\frac{1}{\varepsilon_\mathrm{s}} + \frac{1}{\varepsilon^*}\left(\frac{m_\mathrm{h}}{\Delta m} e^{-r/\rho_\mathrm{h}} - \frac{m_\mathrm{e}}{\Delta m} e^{-r/\rho_\mathrm{e}}\right)\right], \quad (15)$$

in which the bare electron and hole masses have to be used and where Δm is given by $\Delta m = m_\mathrm{h} - m_\mathrm{e}$. Hence we take the statements given above as a reason to propose the following phenomenological potentials for Cu_2O, which are motivated by the formula of Haken and by the formula of Pollmann and Büttner:

$$V^\mathrm{H}(r) = -\frac{e^2}{4\pi\varepsilon_0 r}\left[\frac{1}{\varepsilon_{\mathrm{s}1}} + \frac{1}{2\varepsilon_1^*}(e^{-r/\rho_{\mathrm{h}1}} + e^{-r/\rho_{\mathrm{e}1}}) + \frac{1}{2\varepsilon_2^*}(e^{-r/\rho_{\mathrm{h}2}} + e^{-r/\rho_{\mathrm{e}2}})\right] \quad (16a)$$

and

$$V^\mathrm{PB}(r) = -\frac{e^2}{4\pi\varepsilon_0 r}\left[\frac{1}{\varepsilon_{\mathrm{s}1}} + \frac{1}{\varepsilon_1^*}\left(\frac{m_0}{m_0 - m_\mathrm{e}\gamma_1} e^{-r/\rho_{\mathrm{h}1}} - \frac{m_\mathrm{e}\gamma_1}{m_0 - m_\mathrm{e}\gamma_1} e^{-r/\rho_{\mathrm{e}1}}\right) + \frac{1}{\varepsilon_2^*}\left(\frac{m_0}{m_0 - m_\mathrm{e}\gamma_1} e^{-r/\rho_{\mathrm{h}2}} - \frac{m_\mathrm{e}\gamma_1}{m_0 - m_\mathrm{e}\gamma_1} e^{-r/\rho_{\mathrm{e}2}}\right)\right]. \quad (16b)$$

Here we use

$$\frac{1}{\varepsilon_i^*} = \frac{1}{\varepsilon_{\mathrm{b}i}} - \frac{1}{\varepsilon_{\mathrm{s}i}} \quad (17)$$

and

$$\rho_{\mathrm{e}i} = \sqrt{\frac{\hbar}{2m_\mathrm{e}\omega_{\mathrm{LO}i}}}, \qquad \rho_{\mathrm{h}i} = \sqrt{\frac{\hbar\gamma_1}{2m_0\omega_{\mathrm{LO}i}}}, \quad (18)$$

where the energies of the phonons and the values of the dielectric constants are given by [26]

$$\hbar\omega_{\mathrm{LO}1} = 18.7\ \mathrm{meV}, \qquad \hbar\omega_{\mathrm{LO}2} = 87\ \mathrm{meV}, \quad (19)$$

and

$$\varepsilon_{\mathrm{s}1} = 7.5, \qquad \varepsilon_{\mathrm{b}1} = \varepsilon_{\mathrm{s}2} = 7.11, \qquad \varepsilon_{\mathrm{b}2} = 6.46. \quad (20)$$

As has been done in Ref. [49] for perovskite $CH_3NH_3PbI_3$, we use V^H or V^PB in the Schrödinger equation without an additional fit parameter and find out which of these potentials describes the exciton spectrum of Cu_2O best. Since for the polaron radii ρ_e and $\rho_\mathrm{h} 1.6a \leqslant \rho \leqslant 4.4a$ holds, we expect the Haken or the Pollmann-Büttner potential to have a significant influence on the exciton states with $n \leqslant 2$.

As the Fröhlich coupling constant α^F is small in Cu_2O, i.e., it is $\alpha^\mathrm{F} \lesssim 0.2$ for the two optical phonons and both the electron and the hole [33], the bare electron and hole masses differ from the polaron masses by at most 3%. Hence we can calculate with the bare masses when using V^H.

Besides the frequency dependence of the dielectric function also its momentum dependence becomes important if the exciton radius is on the order of the lattice constant. This momentum dependence of the dielectric function arises from the electronic polarization [26,57].

When treating the excitons of Cu_2O in momentum space, the wave functions of the $n \geqslant 2$ states are localized about $k = 0$ so that for these states the k dependence of ε is not important. However, for the $1S$ state, $a_\mathrm{exc}^{(1S)} \approx a$ holds and thus this state is screened by ε at higher momenta k [26]. Considering the Coulomb interaction for the $1S$ exciton in k space,

$$V(k,\omega) = -\frac{1}{\sqrt{(2\pi)^3}} \frac{e^2}{\varepsilon_0 \varepsilon(k,\omega) k^2}, \quad (21)$$

Kavoulakis *et al.* [26] derived a correction term by assuming

$$\frac{1}{\varepsilon(k,\omega)} \approx \frac{1}{\varepsilon_\mathrm{b} - d(ka)^2} \approx \frac{1}{\varepsilon_\mathrm{b}} + \frac{d(ka)^2}{\varepsilon_\mathrm{b}^2} \quad (22)$$

valid for $E_\mathrm{g}/\hbar \gg \omega \gg \omega_\mathrm{LO}$ with a small unknown constant d. Inserting Eq. (22) in Eq. (21) and Fourier transforming the second expression, one obtains the following correction term to the Coulomb interaction:

$$V_d = -da^2 \frac{e^2}{\varepsilon_0 \varepsilon_\mathrm{b}^2} V_\mathrm{uc}\, \delta(\boldsymbol{r}) = -V_0 V_\mathrm{uc} \delta(\boldsymbol{r}). \quad (23)$$

Following the calculation of Ref. [57] on the dielectric function and using the lowest Γ_8^- conduction band and the highest Γ_7^+ valence band, Kavoulakis *et al.* [26] estimated the value of d to $d \approx 0.18$ [26].

Note that in general a Kronecker delta would appear in Eq. (23) [1]. However, as we treat the exciton problem in the continuum approximation, this Kronecker delta is replaced by the delta function times the volume $V_{uc} = a^3$ of one unit cell. Thus the parameter V_0 has the unit of an energy.

We have already stated above that the Haken potential cannot describe the electron-hole interaction correctly for very small r. Therefore we now assume that the potential (23) is not only due to the momentum dependence of the dielectric function but that it also accounts for deviations from the Haken potential at small r. Hence we will treat V_0 as an unknown fit parameter in the following.

C. Exchange interaction

In the Wannier equation or Hamiltonian of excitons, the exchange interaction is generally not included but regarded as a correction to the hydrogenlike solution [1]. Recently, we have presented a comprehensive discussion of the exchange interaction in Cu_2O [13]. We could show, in accordance with Ref. [26], that corrections to the exchange interaction due to a finite momentum $\hbar\boldsymbol{K}$ of the center of mass of the exciton are negligibly small. Hence only the K independent part of the exchange interaction [13,17,51,58],

$$H_{\mathrm{exch}} = J_0\left(\frac{1}{4} - \frac{1}{\hbar^2}\boldsymbol{S}_{\mathrm{e}}\cdot\boldsymbol{S}_{\mathrm{h}}\right)V_{\mathrm{uc}}\delta(\boldsymbol{r}), \tag{24}$$

needs to be considered. Within the simple hydrogenlike model, the exchange interaction would only affect the nS exciton states as these states have a nonvanishing probability density at $r = 0$. However, when considering the complete valence-band structure, the exciton states with even or with odd values of L are coupled, and thus the exchange interaction will affect the whole even exciton series.

It is well known from experiments that the splitting between the yellow $1S$ ortho and the yellow $1S$ para exciton amounts to about 12 meV [59–61]. Hence we have to choose the value of $\tilde{J}_0$ such that this splitting is reflected in the theoretical spectrum.

D. Summary

Following the explanations given in Secs. III B and III C, the term V_{CCC} in the Hamiltonian of Eq. (5) takes one of the following forms:

$$V^{\mathrm{H}}_{\mathrm{CCC}}(\boldsymbol{r}) = -\frac{e^2}{4\pi\varepsilon_0 r}\left[\frac{1}{2\varepsilon_1^*}(e^{-r/\rho_{\mathrm{h1}}} + e^{-r/\rho_{\mathrm{e1}}}) + \frac{1}{2\varepsilon_2^*}(e^{-r/\rho_{\mathrm{h2}}} + e^{-r/\rho_{\mathrm{e2}}})\right] + \left[-V_0 + J_0\left(\frac{1}{4} - \frac{1}{\hbar^2}\boldsymbol{S}_{\mathrm{e}}\cdot\boldsymbol{S}_{\mathrm{h}}\right)\right]V_{\mathrm{uc}}\delta(\boldsymbol{r}), \tag{25a}$$

$$V^{\mathrm{PB}}_{\mathrm{CCC}}(\boldsymbol{r}) = -\frac{e^2}{4\pi\varepsilon_0 r}\left[\frac{1}{\varepsilon_1^*}\left(\frac{m_0}{m_0 - m_{\mathrm{e}}\gamma_1}e^{-r/\rho_{\mathrm{h1}}} - \frac{m_{\mathrm{e}}\gamma_1}{m_0 - m_{\mathrm{e}}\gamma_1}e^{-r/\rho_{\mathrm{e1}}}\right) + \frac{1}{\varepsilon_2^*}\left(\frac{m_0}{m_0 - m_{\mathrm{e}}\gamma_1}e^{-r/\rho_{\mathrm{h2}}} - \frac{m_{\mathrm{e}}\gamma_1}{m_0 - m_{\mathrm{e}}\gamma_1}e^{-r/\rho_{\mathrm{e2}}}\right)\right]$$
$$+\left[-V_0 + J_0\left(\frac{1}{4} - \frac{1}{\hbar^2}\boldsymbol{S}_{\mathrm{e}}\cdot\boldsymbol{S}_{\mathrm{h}}\right)\right]V_{\mathrm{uc}}\delta(\boldsymbol{r}), \tag{25b}$$

[cf. Eqs. (16a), (16b), (23), and (24)]. Note that while the operators with $\delta(\boldsymbol{r})$ affect only the exciton series with even values of L, the Haken or Pollmann and Büttner potential affect all exciton states [44]. A comparison of our results with the experimental values of Refs. [2,3,17,62,63] will allow us, in Sec. V, to determine the size of the unknown parameters V_0 and J_0.

IV. EIGENVALUES AND OSCILLATOR STRENGTHS

In this section, we describe how the Schrödinger equation corresponding to the Hamiltonian (5) is solved in a complete basis. Furthermore, we discuss how to calculate oscillator strengths for two-photon absorption. An appropriate basis to solve the Schrödinger equation has been presented in detail in Ref. [10]. Hence we recapitulate only the most important points.

As regards the angular momentum part of the basis, we have to consider that the different operators in the Hamiltonian couple the quasispin I, the hole spin S_{h}, and the angular momentum L of the exciton. Hence, we introduce the effective hole spin $J = I + S_{\mathrm{h}}$, the angular momentum $F = L + J$, and the total angular momentum $F_t = F + S_{\mathrm{e}}$. For the radial part of the exciton wave function, we use the Coulomb-Sturmian functions [64]

$$U_{NL}(r) = N^{(\alpha)}_{NL}(2\rho)^L e^{-\rho} L^{2L+1}_N(2\rho) \tag{26}$$

with $\rho = r/\alpha$, an arbitrary convergence or scaling parameter α, the associated Laguerre polynomials $L^m_n(x)$, and a normalization factor

$$N^{(\alpha)}_{NL} = \frac{2}{\sqrt{\alpha^3}}\left[\frac{N!}{(N+L+1)(N+2L+1)!}\right]^{\frac{1}{2}}. \tag{27}$$

The radial quantum number N is related to the principal quantum number n via $n = N + L + 1$. Finally, we use the following ansatz for the exciton wave function

$$|\Psi\rangle = \sum_{NLJFF_tM_{F_t}} c_{NLJFF_tM_{F_t}}|\Pi\rangle, \tag{28a}$$

$$|\Pi\rangle = |N, L; (I, S_{\mathrm{h}})\,J;\ F, S_{\mathrm{e}};\ F_t, M_{F_t}\rangle \tag{28b}$$

with real coefficients c. The parenthesis and semicolons in Eq. (28b) are meant to illustrate the coupling scheme of the spins and the angular momenta. Since the z axis is a fourfold axis, it is sufficient to use only M_{F_t} quantum numbers which differ by ± 4 in Eq. (28).

We now express the Hamiltonian (5) in terms of irreducible tensors [29,65,66]. Inserting the ansatz (28) in the Schrödinger equation $H\Psi = E\Psi$ and multiplying from the left with another basis state $\langle\Pi'|$, we obtain a matrix representation of the Schrödinger equation of the form

$$\boldsymbol{D}\boldsymbol{c} = E\boldsymbol{M}\boldsymbol{c}. \tag{29}$$

The vector $\boldsymbol{c}$ contains the coefficients of the ansatz (28). All matrix elements, which enter the symmetric matrices $\boldsymbol{D}$ and $\boldsymbol{M}$ and which have not been treated in Ref. [10], are given in Appendix D. The generalized eigenvalue problem (29) is finally solved using an appropriate LAPACK routine [67]. The material parameters used in our calculation are listed in Table I.

Since the basis cannot be infinitely large, the values of the quantum numbers are chosen in the following way. For each value of $n = N + L + 1$, we use

$$\begin{aligned} L &= 0, \ldots, n-1, \\ J &= 1/2, 3/2, \\ F &= |L-J|, \ldots, \min(L+J, F_{\max}), \\ F_t &= F - 1/2, F + 1/2, \\ M_{F_t} &= -F_t, \ldots, F_t. \end{aligned} \tag{30}$$

The value $F_{\max}$ and the maximum value of n are chosen appropriately large so that the eigenvalues converge. Additionally, we can use the scaling parameter α to enhance convergence. However, it should be noted that the value of α does not influence the theoretical results for the exciton energies in any way, i.e., the converged results do not depend on the value of α.

Note that the presence of the delta functions in Eq. (25) makes the whole problem more complicated than in Ref. [10] since not only the eigenvalues but also the wave functions at $r = 0$ have to converge. However, for a specific value of α, it is not possible to obtain convergence for all exciton states of interest. Therefore we solve the Schrödinger equation initially without the $\delta(\boldsymbol{r})$ dependent terms. We then select the converged eigenvectors and with these we set up a second generalized eigenvalue problem now including the $\delta(\boldsymbol{r})$ dependent terms. This problem is again solved using an appropriate LAPACK routine [67] and provides the correct converged eigenvalues of the complete Hamiltonian (5).

Having solved the eigenvalue problem, we can use the eigenvectors to determine relative oscillator strengths. The determination of relative oscillator strengths in one-photon absorption has been presented in detail in Refs. [10,14]. While in one photon absorption excitons of symmetry Γ_4^- are dipole-allowed [10], the selection rules for two-photon absorption [70–72] are different and excitons of symmetry Γ_5^+ can be optically excited.

When considering one-photon absorption one generally treats the operator $\boldsymbol{A}\boldsymbol{p}$ with the vector potential $\boldsymbol{A}$ of the radiation field in first order perturbation theory. The dipole operator then transforms according to the irreducible representation D^1 of the full rotation group. In two-photon absorption one needs the operator $\boldsymbol{A}\boldsymbol{p}$ twice and thus the product $D^1 \otimes D^1 = D^0 \oplus D^1 \oplus D^2$ has to be considered [32]. In Cu_2O, the reduction of these irreducible representations by the cubic group O_h has to be considered and one obtains

$$\Gamma_4^- \otimes \Gamma_4^- = \Gamma_1^+ \oplus \Gamma_4^+ \oplus (\Gamma_3^+ \oplus \Gamma_5^+). \tag{31}$$

In two-photon absorption, the spin $S = S_e + S_h = 0$ remains unchanged and the exciton state must have an $L = 0$ component. Hence the correct expression for the relative oscillator strength is given by

$$f_{\text{rel}} \sim \left| \lim_{r \to 0} {}_T\langle 1, M'_{F_t} | \Psi(\boldsymbol{r}) \rangle \right|^2, \tag{32}$$

with the wave function $|\Psi\rangle$ of Eq. (28) and the state $|F_t, M_{F_t}\rangle_T$, which is a short notation for

$$\begin{aligned} &\left|(S_e, S_h)\, S, I;\ I+S, L;\ F_t, M_{F_t}\right\rangle \\ &\quad = \left|(1/2, 1/2)\, 0, 1;\ 1, 0;\ F_t, M_{F_t}\right\rangle. \end{aligned} \tag{33}$$

Note that the coupling scheme of the spins and angular momenta in Eq. (33) given by

$$S_e + S_h = S \quad \rightarrow \quad (I+S) + L = F_t \tag{34}$$

is different from the one of Eq. (28b) due to the requirement that S must be a good quantum number.

It can be shown that the state $|1, M_{F_t}\rangle_T$ transforms according to the irreducible representation Γ_5^+ of O_h [32], for which reason only exciton states of this symmetry can be excited in two-photon absorption. By choosing particular directions of the polarization of the light, e.g., by choosing one photon being polarized in x direction and one photon being polarized in y direction, only one component of the Γ_5^+ exciton states, the xy component, can be excited optically. We consider this case in the following and hence use $M'_{F_t} = 0$ in Eq. (32). Finally, we wish to note that the exciton states of symmetry Γ_5^+ can weakly be observed in one-photon absorption in quadrupole approximation [17].

V. RESULTS AND DISCUSSION

In this section, we determine the values of the parameters J_0 and V_0 and discuss the complete exciton spectrum of Cu_2O. The parameter J_0 describes the strength of the exchange interaction. It is well known that the exchange interaction mainly affects the $1S$ exciton and that the splitting between the ortho and the para exciton state amounts to 11.8 meV [17,59–62]. By choosing

$$J_0 = 0.792 \pm 0.068\ \text{eV}, \tag{35}$$

we obtain the correct value of this splitting irrespective of whether using the Haken or the Pollman-Büttner potential [cf. Eq. (25)].

Figures 4 and 5 show the effect of the correction with the coefficient V_0 on the spectrum for the Haken and the Pollman-Büttner potential, respectively. As can be seen from these figures, the exchange splitting of the $1S$ state hardly changes when varying the value V_0. Hence we can determine V_0 almost independently of J_0.

To find the optimum value of V_0, we compare our results to the energies of the even parity exciton states given in Refs. [9,11,17,62,63,73]. However, we can see from Figs. 4 and 5 that there is no value of V_0 for which all theoretical results take the values of the experimentally determined energies. This is not unexpected since the central-cell corrections are only an attempt to account for the specific properties of the $1S$ exciton within the continuum limit of Wannier excitons and are not an exact description of this exciton state. Hence we do not expect a perfect agreement between theory and experiment.

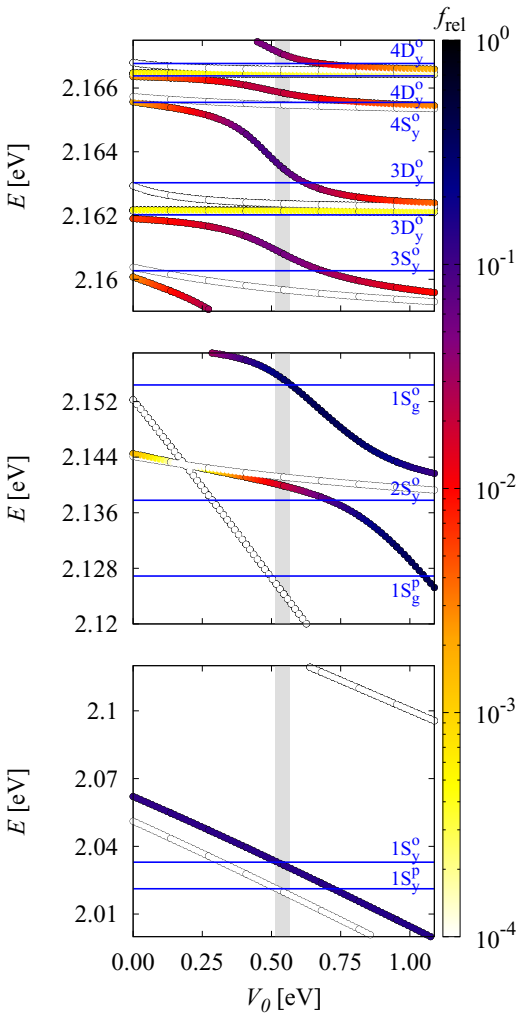

FIG. 4. Behavior of the even exciton states as functions of V_0 when using V^{H}_{CCC} [see Eq. (25a)]. The color bar shows the relative oscillator strengths for two-photon absorption. The blue straight lines denote the position of the dipole-allowed Γ_5^+ S and D exciton states observed in the experiment. We also show the positions of the $1S$ para excitons ($1S^p_{y/g}$). The gray area indicates the optimum range of $V_0 = 0.539 \pm 0.027$ eV, where the ratio of the relative oscillator strengths of the yellow $2S$ and the green $1S$ state amounts to $\sim$16. The effect of the central-cell corrections on the whole even exciton spectrum is evident. For further information see text.

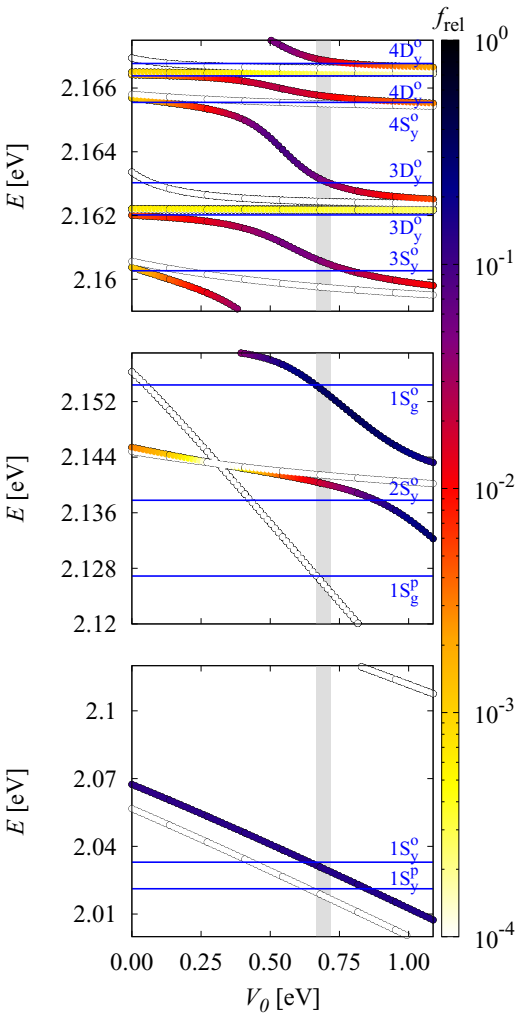

FIG. 5. Same calculation as in Fig. 4 but with V^{PB}_{CCC} [see Eq. (25b)]. One can see only slight differences for the $n = 1$ and $n = 2$ exciton states when comparing the results to Fig. 4. The gray area indicates the optimum range of $V_0 = 0.694 \pm 0.027$ eV.

Small deviations from the experimental values could also be explained by small uncertainties in the Luttinger parameters γ_i, η_i [9,10] or the band-gap energy [2] as well as by a finite temperature or small strains in the crystal. On the other hand, it is also possible that the experimental values are affected by uncertainties. This can be seen, e.g., when comparing the slightly different experimental results of Refs. [9,11,63].

Note that the almost perfect agreement between theoretical and experimental results in Refs. [17,25] could only be obtained by taking also γ_1', μ' and Δ as fit parameters to the experiment. However, these parameters are connected to the band structure in Cu_2O [33] and cannot be chosen arbitrarily [3,10].

It can be seen from Figs. 4 and 5 that the oscillator strength of the exciton state at $E \approx 2.143$ eV changes rapidly with increasing V_0. From the experimental results of Refs. [17,25], we know that the two exciton states at $E = 2.1378$ and 2.1544 eV are well separated from the other exciton states and that the phonon background is small. Hence the ratio of the relative two-photon oscillator strengths can be calculated quite accurately to $\sim$16.

We now choose the value of V_0 such that the ratio of the calculated two-photon oscillator strengths reaches the same value and obtain

$$V_0 = 0.539 \pm 0.027 \text{ eV} \tag{36}$$

when using the Haken potential [cf. Eq. (25a)] or

$$V_0 = 0.694 \pm 0.027 \text{ eV} \tag{37}$$

when using the Pollmann-Büttner potential [cf. Eq. (25b)]. Note that the error bars for V_0 are chosen such that the ratio of the oscillator strengths lies between 14 and 18.

Having determined the most suitable values of V_0 and J_0, we can now turn our attention to the exciton Bohr radius $a_{\mathrm{exc}}^{(1S)}$ of the $1S$ orthoexciton and to the correct assignment of the $n = 2$ exciton states. To determine the radius $a_{\mathrm{exc}}^{(1S)}$, we evaluate

$$\langle\Psi|r|\Psi\rangle = \sum_{N'} \sum_{NLJFF_tM_{F_t}} c_{N'LJFF_tM_{F_t}} c_{NLJFF_tM_{F_t}} \times \sum_{j=-2}^{2} \frac{\alpha(R_2)_{NL}^{j}}{N+L+j+1} \delta_{N',\,N+j} \tag{38}$$

with the wave function Ψ of Eq. (28) and compare the result with the formula [74]

$$\langle r\rangle = \tfrac{1}{2} a_{\mathrm{exc}}^{(1S)} [3n^2 - L(L+1)] \tag{39}$$

known from the hydrogenlike model, where we set $n = 1$ and $L = 0$. Note that the function $(R_2)_{NL}^{j}$ in Eq. (38) is taken from the recursion relations of the Coulomb-Sturmian functions in the Appendix of Ref. [10]. We obtain

$$a_{\mathrm{exc}}^{(1S)} \approx 0.793\ \mathrm{nm} \approx 1.86\, a \tag{40}$$

when using the Haken potential or

$$a_{\mathrm{exc}}^{(1S)} \approx 0.810\ \mathrm{nm} \approx 1.90\, a \tag{41}$$

when using the Pollmann-Büttner potential. In both cases the radius of the $1S$ orthoexciton is large enough that the corrections to the kinetic energy discussed in Sec. III A can certainly be neglected.

Let us now proceed to the correct assignment of the $n = 2$ exciton states. Since in the investigation of Uihlein *et al.* [17,25], the wrong values for the Luttinger parameters were used (cf. Ref. [10]), it is not clear whether the state at $E = 2.1544$ eV can still be assigned as the yellow $2S$ orthoexciton state and the state at $E = 2.1378$ eV as the green $1S$ orthoexciton state when using the correct Luttinger parameters.

To demonstrate from which hydrogenlike states, the experimentally observed exciton states originate, we find it instructive to start from the hydrogenlike spectrum with almost all material parameters set to zero and then increase these material parameters successively to their true values. This is shown in Fig. 6.

At first all material parameters except for γ_1' are set to zero, so that a true hydrogenlike spectrum is obtained, where the yellow (y) and green (g) exciton states are degenerate. This spectrum is shown in the panel (a) of Fig. 6. When increasing the spin-orbit coupling constant Δ in Fig. 6(a), the degeneracy between the green and the yellow exciton series is lifted. The increase of the Luttinger parameters μ' and δ' in the panels (b) and (c) furthermore lifts the degeneracy between the exciton states of different angular momentum L. The Haken potential does not change degeneracies but slightly lowers the energy of the exciton states in Fig. 6(d). The exchange energy described by the constant J_0 lifts the degeneracy between ortho and paraexciton states in Fig. 6(e). As the operator $\delta(\boldsymbol{r})$ affects only the states of even parity (blue lines), the energy of the odd exciton states (red lines) remains unchanged in Fig. 6(f). Note that we increase Δ in two steps to its true value of $\Delta = 0.131$ eV for reasons of clarity. Hence, at the bottom of Fig. 6(g), all material values have been increased to their true values. For a comparison, we show in panel (h) the position of the experimentally observed states. Following the exciton states from panel (a) to (g), it is possible to assign them with the notation $nL_{\mathrm{y/g}}^{\mathrm{p/o}}$, where the upper index denotes a para or an ortho exciton state and the lower index a yellow or a green state.

The results presented in Fig. 6 suggest to assign the exciton state at $E = 2.1378$ eV to the green $1S$ orthoexciton state. However, one can observe an anticrossing between the green $1S$ state and the yellow $2S$ state, which is indicated by a green arrow in Fig. 6(g). Hence, the assignment has to be changed. As a proof, we can calculate the percentage of the $J = 3/2$ component of these states, i.e., their green part, by evaluating

$$\mathrm{gp} = \langle\Psi|P|\Psi\rangle \tag{42}$$

with the projection operator

$$P = \sum_{M_J=-3/2}^{3/2} \left|\frac{3}{2}, M_J\right\rangle\!\left\langle\frac{3}{2}, M_J\right| \tag{43}$$

and the exciton wave function $|\Psi\rangle$ (see also Appendix C).

The green part gp of the state at $E \approx 2.1544$ eV is distinctly higher (gp $\approx 40\%$) than the green part of the exciton state at $E \approx 2.1378$ eV (gp $\approx 11\%$). However, since also gp $\approx 40\%$ is significantly smaller than one, we see that the assignment of this exciton state as the ground state of the green series is questionable and shows the significant deviations from the hydrogenlike model. The green $1S$ exciton state is distributed over the yellow states. Note that in Ref. [17] also the state of higher energy had a larger green part than the state of lower energy. However, in Fig. 2 of Ref. [17] the assignment is reversed since the limit of $\mu' \to 0$ was used to designate the states. It seems obvious that a similar anticrossing between the green $1S$ state and the yellow $2S$ state was disregarded. A considerable effect of the interaction between the green and yellow series is the change in the oscillator strength of the states. The oscillator strength of the $2S_y$ state is much smaller than expected when assuming two independent, i.e., green and yellow, series [17,25] (cf. also Tables III and IV).

For reasons of completeness, we give the size of the green $1S$ and the yellow $2S$ state by evaluating Eq. (38). Since these states are strongly mixed and a correct assignment with a principal quantum number n is not possible, we do not use the formula (39). We obtain

$$\langle r\rangle(2S_y) \approx 4.32\ \mathrm{nm} \approx 10.1\, a, \tag{44a}$$

$$\langle r\rangle(1S_g) \approx 5.32\ \mathrm{nm} \approx 12.5\, a, \tag{44b}$$

when using the Haken potential or

$$\langle r\rangle(2S_y) \approx 4.39\ \mathrm{nm} \approx 10.3\, a, \tag{45a}$$

$$\langle r\rangle(1S_g) \approx 4.09\ \mathrm{nm} \approx 9.58\, a, \tag{45b}$$

when using the Pollmann-Büttner potential. We see that in both cases the values of $\langle r\rangle$ for the green $1S$ and the yellow $2S$ state are of the same size. This is expected due to the strong mixing of both states.

The resonance of the green $1S$ state with the yellow exciton series and the mixing of all even exciton states via the cubic

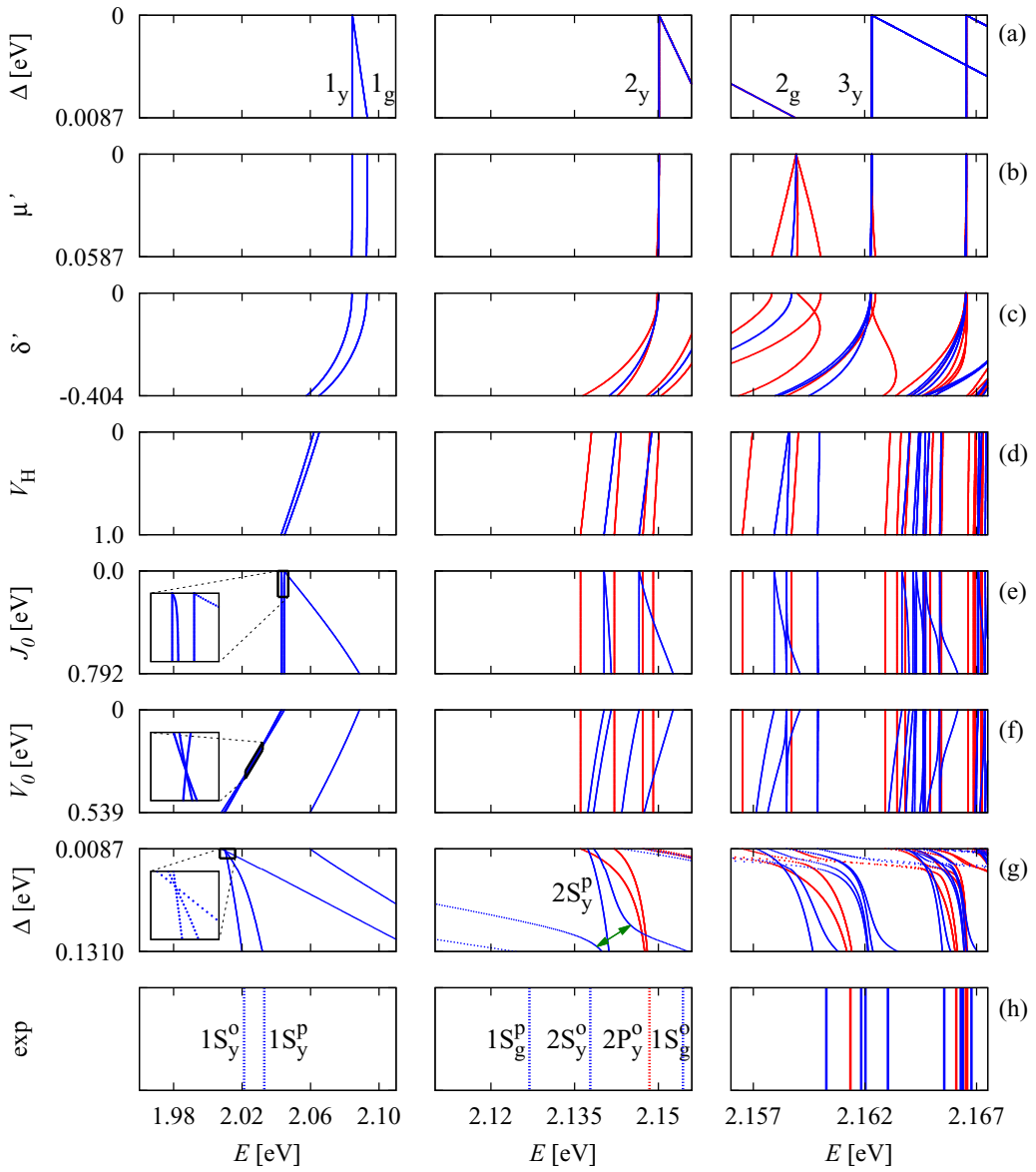

FIG. 6. Exciton spectrum of the even (blue) and odd (red) exciton states when increasing all material parameters from zero (top) to their correct values (bottom) and using V^{H}_{CCC} [cf. Eq. (25b)]. If all material parameters except for γ_1' are set to zero, one obtains a hydrogenlike spectrum, for which the yellow (y) and green (g) exciton states are degenerate [$\Delta = 0$ in (a)]. When increasing the spin-orbit coupling constant Δ, this degeneracy is lifted and the green exciton states are shifted towards higher energies (a). Note that we increase Δ in two steps to its true value of $\Delta = 0.131$ eV for reasons of clarity. One can then follow these states from (b) to (g). Since the effect of the parameters η_1', ν and τ on the exciton spectrum is small they are immediately set from zero to their correct values between (c) and (d). In (g) and (h), the para and orthoexciton states are denoted by an upper index p and o. The final results at the bottom of (g), which are also listed in Table III, can then be compared to the position of the exciton states obtained from experiments (h). Note that due to the marked anticrossing [green arrow in the second panel of (g)] the assignment of the green $1S$ state and the yellow $2S$ state changes.

band structure leads to an admixture of D and G states to the green $1S$ state. Hence the three Γ_5^+ states which we assigned with $1S_g$ are elliptically deformed and invariant only under the subgroup D_{4h} of O_h [10,32]. The lower symmetry of the envelope function allows for a smaller mean distance between electron and hole in a specific direction, which leads to a gain of energy due to the Coulomb interaction [10]. As regards the xy component, the symmetry axis of the according subgroup D_{4h} is the z axis of the crystal. Since for this state the expectation values $\langle\Psi|x^2|\Psi\rangle$ and $\langle\Psi|y^2|\Psi\rangle$ are identical, we can calculate the semiprincipal axes of the elliptically deformed state by evaluating

$$\begin{aligned}\langle\Psi|x^2|\Psi\rangle &= \langle\Psi|\frac{1}{2}(r^2 - z^2)|\Psi\rangle \\ &= \sum_{N'L'J'F'F_t'M_{F_t}'} \sum_{NLJFF_tM_{F_t}} c_{N'L'J'F'F_t'M_{F_t}'} c_{NLJFF_tM_{F_t}} \\ &\quad \times \alpha^2 \langle\Pi'|\frac{1}{3}r^2 - \frac{1}{3\sqrt{6}} X_0^{(2)}|\Pi\rangle \end{aligned} \tag{46}$$

TABLE II. Decomposition of the irreducible representations of the rotation group or the angular momentum states by the cubic group O_h. Note that the quasispin I already enters the momentum F via J. The irreducible representations denote the symmetry of the envelope function (L), the combined symmetry of envelope and hole (F) or the complete symmetry of the exciton (F_t).

L	$F = L + J\ (J = \frac{1}{2})$	$F_t = F + S_e$
$0\ \Gamma_1^+$	$\frac{1}{2}\ \Gamma_7^+$	$\begin{matrix}0 & \Gamma_2^+\\ 1 & \Gamma_5^+\end{matrix}$
$1\ \Gamma_4^-$	$\frac{1}{2}\ \Gamma_7^-$	$\begin{matrix}0 & \Gamma_2^-\\ 1 & \Gamma_5^-\end{matrix}$
	$\frac{3}{2}\ \Gamma_8^-$	$\begin{matrix}1 & \Gamma_4^-\\ 2 & \Gamma_3^- \oplus \Gamma_5^-\end{matrix}$
$2\ \Gamma_3^+ \oplus \Gamma_5^+$	$\frac{3}{2}\ \Gamma_8^+$	$\begin{matrix}1 & \Gamma_5^+\\ 2 & \Gamma_3^+ \oplus \Gamma_4^+\end{matrix}$
	$\frac{5}{2}\ \Gamma_6^+ \oplus \Gamma_8^+$	$\begin{matrix}2 & \Gamma_3^+ \oplus \Gamma_4^+\\ 3 & \Gamma_1^+ \oplus \Gamma_4^+ \oplus \Gamma_5^+\end{matrix}$
$3\ \Gamma_1^- \oplus \Gamma_4^- \oplus \Gamma_5^-$	$\frac{5}{2}\ \Gamma_6^- \oplus \Gamma_8^-$	$\begin{matrix}2 & \Gamma_3^- \oplus \Gamma_4^-\\ 3 & \Gamma_1^- \oplus \Gamma_4^- \oplus \Gamma_5^-\end{matrix}$
	$\frac{7}{2}\ \Gamma_6^- \oplus \Gamma_7^- \oplus \Gamma_8^-$	$\begin{matrix}3 & \Gamma_2^- \oplus \Gamma_4^- \oplus \Gamma_5^-\\ 4 & \Gamma_2^- \oplus \Gamma_3^- \oplus \Gamma_4^- \oplus \Gamma_5^-\end{matrix}$
L	$F = L + J\ (J = \frac{3}{2})$	$F_t = F + S_e$
$0\ \Gamma_1^+$	$\frac{3}{2}\ \Gamma_8^+$	$\begin{matrix}1 & \Gamma_5^+\\ 2 & \Gamma_3^+ \oplus \Gamma_4^+\end{matrix}$

and

$$\langle \Psi | z^2 | \Psi \rangle = \sum_{N'L'J'F'F_t'M_{F_t}'} \sum_{NLJFF_tM_{F_t}} c_{N'L'J'F'F_t'M_{F_t}'} c_{NLJFF_tM_{F_t}} \times \alpha^2 \langle \Pi' | \frac{1}{3}\sqrt{\frac{2}{3}} X_0^{(2)} + \frac{1}{3} r^2 | \Pi \rangle \tag{47}$$

with the wave function Ψ of Eq. (28) and the matrix elements $\langle \Pi' | X_0^{(2)} | \Pi \rangle$ and $\langle \Pi' | r^2 | \Pi \rangle$ listed in the Appendix of Ref. [14]. We obtain

$$\begin{aligned} \langle x^2 \rangle &\approx 116.4\, a^2, \\ \langle z^2 \rangle &\approx 29.9\, a^2, \end{aligned} \tag{48}$$

when using the Haken potential or

$$\begin{aligned} \langle x^2 \rangle &\approx 68.6\, a^2, \\ \langle z^2 \rangle &\approx 25.1\, a^2, \end{aligned} \tag{49}$$

when using the Pollmann-Büttner potential. The significant differences in $\langle x^2 \rangle$ and $\langle z^2 \rangle$ show again the strong resonance of the green $1S$ state with the yellow series as well as the strong admixture of states with $L \geqslant 2$. We finally want to note that, due to the coupling of the yellow and green series, the green $1S$ has to be regarded as an excited state in the complete exciton spectrum and not as the ground state of the green series. In particular, the green $1S$ state is orthogonal to the true ground state of the complete spectrum, i.e., to the yellow $1S$ state.

Let us now discuss the other exciton states. To determine the number of para and orthoexciton states as well as their degeneracies for the different values of L, one can use group theoretical considerations. In the spherical approximation, in which the cubic part of the Hamiltonian is neglected ($\delta' = 0$), the momentum $F = J + L$ is a good quantum number for the states of negative parity since the exchange interaction does not act on these states. The states of positive parity can be classified by the total momentum $F_t = F + S_e$ in the spherical approximation.

If the complete cubic Hamiltonian is treated, the reduction of the irreducible representations D^F or D^{F_t} of the rotation group by the cubic group O_h has to be considered [75]. This is shown in Table II. As has already been stated in Ref. [10], a normal spin one transforms according to the irreducible representation Γ_4^+ of the cubic group, whereas the quasispin I transforms according to $\Gamma_5^+ = \Gamma_4^+ \otimes \Gamma_2^+$. Therefore one has to include the additional factor Γ_2^+ when determining the symmetry of an exciton state [3,10,17]. This symmetry is given by the symmetry of the envelope function, the valence band, and the conduction band:

$$\Gamma_{exc} = \Gamma_{env} \otimes \Gamma_v \otimes \Gamma_c. \tag{50}$$

Only states of symmetry Γ_4^- are allowed in one-photon absorption and only states of symmetry Γ_5^+ are allowed in two-photon absorption. Hence we see from Table II that there are at the most one P state and four F states or one S and two D states for each principal quantum number n, which can be observed in experiments.

Since the exchange interaction does not act on the exciton states with negative parity, one can use the irreducible representations of the second column of Table II to classify these exciton states [3]. For the exciton states of positive parity the irreducible representations of the third column are needed. Note that the cubic part of the Hamiltonian mixes the S and D exciton states of symmetry Γ_5^+. Hence the exchange interaction acts only on the D excitons of symmetry Γ_5^+ via their S component. The degeneracies between the D states of symmetry Γ_3^+ and Γ_4^+ or Γ_1^+ and Γ_4^+ is not lifted, respectively (cf. the third column of Table II).

Since neither J nor F are good quantum numbers due to the cubic symmetry of our Hamiltonian, we do not use the nomenclature $n^{2J+1}L_F$ of Refs. [17,25]. Although L is likewise no good quantum number, the assignment of the exciton states by using S, P, D, F and G to denote the angular momentum is still common (see, e.g., Refs. [3,9]). Hence we feel obliged to classify the states by introducing the notation $nL_{y/g}$ for comparison with other works but also stress that this is generally not instructive due to the large deviations from the hydrogenlike model (cf. also Ref. [10]). By the index y or g we denote the yellow or the green exciton series, respectively. To be more correct, we will also give the symmetry of the exciton states in terms of the irreducible representations of Table II. These symmetries can be determined by regarding the eigenvectors of the generalized eigenvalue problem (29) [10].

In Tables III and IV, we now give a direct comparison between experimental and theoretical exciton energies for all states with $n \leqslant 5$. One can see that the results with the

TABLE III. Comparison of calculated energies E_{theor} to experimental values E_{exp} (references given behind experimental values) when using the central-cell corrections with the Haken potential (25a). Note that we use $E_g = 2.17202$ eV instead of $E_g = 2.17208$ eV [2] to obtain a better agreement. The assignment of the states in the first column is motivated by Fig. 6 but is generally not instructive due to the large deviations from the hydrogenlike model. Hence we also give the symmetry of the states. In the case of the P and F excitons, we do not give the symmetry of the complete exciton state but only the combined symmetry of envelope and hole. As regards the $5G$ excitons, we only give the average energy of the states of symmetry Γ_5^+. The value in the fourth column gives the relative oscillator strength in one-photon absorption (nP, nF excitons; see Ref. [10]) or in two-photon absorption [nS, nD, nG excitons; see Eq. (32)]. Note that due to the interaction with the $1S_g$ state the oscillator strength of the $2S_y$ state is much smaller than expected when assuming two independent, i.e., green and yellow, series. The value in the last column indicates the percentage of the $J = 3/2$ component of the state, i.e., the green part. Note that due to the interaction between the yellow and the green exciton series the green $1S$ state is spread over several yellow exciton states. The green states with $n \geqslant 2$ are located far above the states listed here.

State		E_{exp} (eV)	E_{theor} (eV)	f_{rel}	gp (%)	State		E_{exp} (eV)	E_{theor} (eV)	f_{rel}	gp (%)
$1S_y$	Γ_2^+	2.0212 [62]	2.0200	–	5.49	$4D_y$	Γ_3^+,Γ_4^+	2.16629 [11,63]	2.16644	–	0.19
$1S_y$	Γ_5^+	2.0330 [17]	2.0320	26.60	7.22	$4D_y$	Γ_5^+	2.16638 [11,63]	2.16645	0.07	0.19
						$4D_y$	Γ_1^+,Γ_4^+	–	2.16646	–	0.16
$1S_g$	Γ_3^+,Γ_4^+	2.1269 [73]	2.1245	–	71.62	$4F_y$	Γ_7^-	–	2.16653	–	0.12
						$4F_y$	Γ_8^-	2.16652 [3]	2.16654	0.066	0.10
$2S_y$	Γ_5^+	2.1378 [17]	2.1399	3.55	10.88	$4F_y$	Γ_8^-	2.16654 [3]	2.16656	0.002	0.08
$2S_y$	Γ_2^+	–	2.1412	–	1.43	$4F_y$	Γ_6^-	2.16654 [3]	2.16657	0.010	0.08
$2P_y$	Γ_8^-	2.1484 [2]	2.1475	351.4	1.91	$4F_y$	Γ_6^-	2.16658 [3]	2.16660	0.011	0.06
$2P_y$	Γ_7^-	–	2.1480	–	1.30	$4D_y$	Γ_3^+,Γ_4^+	–	2.16658	–	0.22
						$4D_y$	Γ_5^+	2.16677 [11,63]	2.16704	6.86	3.67
$1S_g$	Γ_5^+	2.1544 [17]	2.1553	56.01	36.88						
						$5S_y$	Γ_2^+	–	2.16798	–	0.10
$3S_y$	Γ_2^+	–	2.15967	–	0.48	$5S_y$	Γ_5^+	2.16801 [11,63]	2.16816	2.02	0.81
$3S_y$	Γ_5^+	2.16027 [11,63]	2.16080	10.34	4.49	$5P_y$	Γ_8^-	2.16829 [2]	2.16825	32.82	0.25
$3P_y$	Γ_8^-	2.16135 [2]	2.16119	147.3	0.93	$5P_y$	Γ_7^-	–	2.16830	–	0.18
$3P_y$	Γ_7^-	–	2.16141	–	0.63	$5D_y$	Γ_3^+,Γ_4^+	2.16841 [11,63]	2.16846	–	0.11
$3D_y$	Γ_3^+,Γ_4^+	2.16183 [11,63]	2.16213	–	0.31	$5D_y$	Γ_5^+	2.16846 [11,63]	2.16846	0.05	0.12
$3D_y$	Γ_5^+	2.16202 [11,63]	2.16215	0.09	0.30	$5D_y$	Γ_1^+,Γ_4^+	–	2.16847	–	0.10
$3D_y$	Γ_1^+,Γ_4^+	–	2.16217	–	0.25	$5F_y$	Γ_7^-	–	2.16850	–	0.09
$3D_y$	Γ_3^+,Γ_4^+	–	2.16237	–	0.46	$5F_y$	Γ_8^-	2.16851 [3]	2.16850	0.069	0.07
$3D_y$	Γ_5^+	2.16303 [11,63]	2.16348	15.04	8.49	$5F_y$	Γ_8^-	2.16852 [3]	2.16852	0.000	0.06
						$5F_y$	Γ_6^-	2.16852 [3]	2.16852	0.002	0.06
$4S_y$	Γ_2^+	–	2.16547	–	0.21	$5F_y$	Γ_6^-	2.16855 [3]	2.16855	0.001	0.04
$4S_y$	Γ_5^+	2.16555 [11,63]	2.16584	3.79	1.53	$5D_y$	Γ_3^+,Γ_4^+	–	2.16854	–	0.11
$4P_y$	Γ_8^-	2.16609 [2]	2.16604	67.43	0.45	$5\bar{G}_y$	Γ_5^+	–	2.16855	0.00	0.03
$4P_y$	Γ_7^-	–	2.16614	–	0.32	$5D_y$	Γ_5^+	2.16860 [11,63]	2.16879	4.30	2.22

Haken potential listed in Table III show a better agreement with the experimental values than the results with the Pollmann-Büttner potential listed in Table IV. Hence we have chosen the central-cell corrections with the Haken potential for the calculation of Fig. 6.

The Haken potential or the Pollmann-Büttner potential also slightly affects the odd exciton series and especially the $2P$ exciton state. These potentials shift the energy of the Γ_4^- (resp. Γ_8^-) $2P$ exciton state by an amount of 210 μeV (Haken) or 880 μeV (Pollmann-Büttner) towards lower energies.

TABLE IV. Same comparison as in Table III but when using the central-cell corrections with the Pollmann-Büttner potential (25b). Especially for the states with $n < 3$ differences in the calculated energies can be observed when using the different corrections (25a) or (25b). Note that for each n the relative oscillator strength of one nD state is larger than the relative oscillator strengths of the nS state in accordance with the experimental results of Ref. [17].

State		E_{exp} (eV)	E_{theor} (eV)	f_{rel}	gp (%)	State		E_{exp} (eV)	E_{theor} (eV)	f_{rel}	gp (%)
$1S_y$	Γ_2^+	2.0212 [62]	2.0180	–	5.49	$4D_y$	Γ_3^+,Γ_4^+	2.16629 [11,63]	2.16646	–	0.17
$1S_y$	Γ_5^+	2.0330 [17]	2.0300	27.90	6.83	$4D_y$	Γ_5^+	2.16638 [11,63]	2.16647	0.53	0.18
						$4D_y$	Γ_1^+,Γ_4^+	–	2.16648	–	0.15
$1S_g$	Γ_3^+,Γ_4^+	2.1269 [73]	2.1254	–	65.53	$4F_y$	Γ_7^-	–	2.16653	–	0.12
						$4F_y$	Γ_8^-	2.16652 [3]	2.16654	0.078	0.10
$2S_y$	Γ_5^+	2.1378 [17]	2.1401	4.22	11.16	$4F_y$	Γ_8^-	2.16654 [3]	2.16657	0.002	0.08
$2S_y$	Γ_2^+	–	2.1414	–	1.31	$4F_y$	Γ_6^-	2.16654 [3]	2.16657	0.009	0.08
$2P_y$	Γ_8^-	2.1484 [2]	2.1482	292.3	1.72	$4F_y$	Γ_6^-	2.16658 [3]	2.16660	0.010	0.05
$2P_y$	Γ_7^-	–	2.1486	–	1.20	$4D_y$	Γ_3^+,Γ_4^+	–	2.16661	–	0.19
						$4D_y$	Γ_5^+	2.16677 [11,63]	2.16686	3.24	1.82
$1S_g$	Γ_5^+	2.1544 [17]	2.1535	65.25	42.41						
						$5S_y$	Γ_2^+	–	2.16800	–	0.09
$3S_y$	Γ_2^+	–	2.15974	–	0.44	$5S_y$	Γ_5^+	2.16801 [11,63]	2.16811	1.17	0.48
$3S_y$	Γ_5^+	2.16027 [11,63]	2.16053	7.83	3.29	$5P_y$	Γ_8^-	2.16829 [2]	2.16829	28.17	0.24
$3P_y$	Γ_8^-	2.16135 [2]	2.16138	125.9	0.86	$5P_y$	Γ_7^-	–	2.16834	–	0.17
$3P_y$	Γ_7^-	–	2.16158	–	0.60	$5D_y$	Γ_3^+,Γ_4^+	2.16841 [11,63]	2.16847	–	0.10
$3D_y$	Γ_3^+,Γ_4^+	2.16183 [11,63]	2.16217	–	0.28	$5D_y$	Γ_5^+	2.16846 [11,63]	2.16847	0.04	0.12
$3D_y$	Γ_5^+	2.16202 [11,63]	2.16219	0.07	0.29	$5D_y$	Γ_1^+,Γ_4^+	–	2.16848	–	0.09
$3D_y$	Γ_1^+,Γ_4^+	–	2.16221	–	0.24	$5F_y$	Γ_7^-	–	2.16850	–	0.09
$3D_y$	Γ_3^+,Γ_4^+	–	2.16243	–	0.41	$5F_y$	Γ_8^-	2.16851 [3]	2.16851	0.078	0.07
$3D_y$	Γ_5^+	2.16303 [11,63]	2.16308	8.42	4.87	$5F_y$	Γ_8^-	2.16852 [3]	2.16852	0.000	0.06
						$5F_y$	Γ_6^-	2.16852 [3]	2.16853	0.001	0.06
$4S_y$	Γ_2^+	–	2.16550	–	0.19	$5F_y$	Γ_6^-	2.16855 [3]	2.16855	0.001	0.04
$4S_y$	Γ_5^+	2.16555 [11,63]	2.16575	2.45	0.98	$5D_y$	Γ_3^+,Γ_4^+	–	2.16855	0.00	0.03
$4P_y$	Γ_8^-	2.16609 [2]	2.16612	58.29	0.43	$5\bar{G}_y$	Γ_5^+	–	2.16856	–	0.07
$4P_y$	Γ_7^-	–	2.16621	–	0.31	$5D_y$	Γ_5^+	2.16860 [11,63]	2.16868	1.68	0.92

VI. SUMMARY AND OUTLOOK

We have treated the exciton spectrum of Cu_2O considering the complete valence-band structure, the exchange interaction, and the central-cell corrections. A thorough discussion of the central-cell corrections revealed that only the frequency and momentum dependence of the dielectric function $\varepsilon(k,\omega)$ have to be accounted for. Due to the estimated size of the $1S$ exciton Bohr radius, corrections to the kinetic energy can be neglected. Hence only the two parameters V_0 and J_0 are decisive for the relative position of the exciton states. While J_0 describes the splitting of the exciton states into ortho and para components, V_0 changes the relative energy of the states but leaves this splitting between ortho and para components of the same exciton state almost unchanged. Hence these parameters could be determined almost independently. This means that our results are not very sensitive to the choice of the parameters used. Instead, there is only one combination of both parameters J_0 and V_0 given in Eqs. (35)–(37), for which our results are in good agreement with the experiment.

We have shown that the central-cell corrections considerably affect the complete even exciton series since the valence-band structure couples the $1S$ state to higher exciton states. The frequency dependence of the dielectric function also slightly affects the odd exciton series and lowers, in particular, the energy of the $2P$ exciton state. Furthermore, we have demonstrated that due to the coupling of the yellow

and the green exciton series the green $1S$ exciton state is distributed over all yellow states.

In contrast to earlier works [11], we have presented a closed theory of the complete exciton series in Cu_2O, where we explicitly give the correction potentials (25a) or (25b). Hence the introduction of quantum defects or the introduction of different exchange parameters for different exciton states, which take the effect of the central cell corrections into account only phenomenologically, is redundant [9,11].

The results of our theory show a very good agreement with experimental values (see Table III). Therefore we are confident that an according extension of our theory will allow for the calculation of exciton spectra in Cu_2O in electric or in combined electric and magnetic fields.

ACKNOWLEDGMENTS

F.S. is grateful for support from the Landesgraduiertenförderung of the Land Baden-Württemberg. We thank J. Heckötter, M. Bayer, D. Fröhlich, M. Aßmann, and D. Dizdarevic for helpful discussions.

APPENDIX A: p^4 TERMS

As has already been stated in Sec. III A, the terms of the fourth power of $\boldsymbol{p}$ span a fifteen dimensional space with the basis functions

$$p_i^4, \quad p_i^3 p_j, \quad p_i^2 p_j^2, \quad p_i p_j p_k^2 \tag{A1}$$

with $i,j,k \in \{1,2,3\}$ and $i \neq j \neq k \neq i$. The six linear combinations of p^4 terms (including the quasispin I), which transform according to Γ_1^+ [32] read in terms of irreducible tensors

$$\begin{array}{lcl} \text{(I)} & : & p^4, \\ \text{(II)} & : & P^{(4)}(\Gamma_1^+), \\ \text{(III)} & : & p^2(P^{(2)} \cdot I^{(2)}), \\ \text{(IV)} & : & p^2[P^{(2)} \times I^{(2)}]^{(4)}(\Gamma_1^+), \\ \text{(V)} & : & [P^{(4)} \times I^{(2)}]^{(4)}(\Gamma_1^+), \\ \text{(VI)} & : & [P^{(4)} \times I^{(2)}]^{(6)}(\Gamma_1^+), \end{array} \tag{A2a}$$

with

$$T^{(4)}(\Gamma_1^+) = \sqrt{\frac{5}{24}} \sum_{k=\pm 4} T_k^{(4)} + \sqrt{\frac{7}{12}} T_0^{(4)} \tag{A3a}$$

and

$$T^{(6)}(\Gamma_1^+) = -\frac{\sqrt{7}}{4} \sum_{k=\pm 4} T_k^{(6)} + \frac{1}{\sqrt{8}} T_0^{(6)}. \tag{A3b}$$

One can choose appropriate linear combinations of the states (I)–(VI):

$$\frac{1}{5}\text{(I)} - \frac{1}{3\sqrt{30}}\text{(II)} = \left[p_1^2 p_2^2 + \text{c.p.}\right], \tag{A4a}$$

$$\frac{2}{3}\hbar^2\text{(I)} + \frac{2}{45}\text{(III)} + \frac{1}{18}\sqrt{\frac{24}{5}}\text{(IV)} = \boldsymbol{p}^2\left[p_1^2 \boldsymbol{I}_1^2 + \text{c.p.}\right], \tag{A4b}$$

$$\frac{1}{30}\text{(III)} - \frac{1}{36}\sqrt{\frac{24}{5}}\text{(IV)} = \boldsymbol{p}^2[p_1 p_2 \{\boldsymbol{I}_1, \boldsymbol{I}_2\} + \text{c.p.}], \tag{A4c}$$

$$\frac{6}{5}\hbar^2\text{(I)} - \frac{8}{9\sqrt{30}}\hbar^2\text{(II)} - \frac{4}{27}\sqrt{\frac{7}{11}}\text{(V)} + \frac{1}{9}\sqrt{\frac{14}{33}}\text{(VI)} = \left[\left(p_1^4 + 6p_2^2 p_3^2\right)\boldsymbol{I}_1^2 + \text{c.p.}\right] \tag{A4d}$$

$$-\frac{1}{18}\sqrt{\frac{7}{11}}\text{(V)} - \frac{1}{9}\sqrt{\frac{14}{33}}\text{(IV)} = \left[\left(p_1^2 + p_2^2 - 6p_3^2\right) p_1 p_2 \{\boldsymbol{I}_1, \boldsymbol{I}_2\} + \text{c.p.}\right] \tag{A4e}$$

with $\{a,b\} = \frac{1}{2}(ab + ba)$ and c.p. denoting cyclic permutation. These linear combinations enter the generalized expressions of the kinetic energy of the hole and the electron in Sec. III A.

APPENDIX B: OSCILLATOR STRENGTHS

We now give the formula for the expression

$$\lim_{r \to 0} {}_T\langle 1, M'_{F_t} | \Psi(\boldsymbol{r}) \rangle, \tag{B1}$$

which is needed for the evaluation of the relative oscillator strength f_{rel} (32) in two photon absorption experiments. Using the wave function of Eq. (28), we find

$$\begin{aligned} \lim_{r \to 0} {}_T\langle 1, M'_{F_t} | \Psi(\boldsymbol{r}) \rangle = \sum_{NFF_t} \sum_{M_{S_e}} c_{N0FFF_tM'_{F_t}} \sqrt{\frac{2}{\alpha^3}} (-1)^{F-2M_{S_e}+\frac{1}{2}} [(2F+1)(2F_t+1)]^{\frac{1}{2}} \\ \times \begin{pmatrix} F & \frac{1}{2} & F_t \\ M'_{F_t} - M_{S_e} & M_{S_e} & -M'_{F_t} \end{pmatrix} \begin{pmatrix} 1 & \frac{1}{2} & F \\ M'_{F_t} & -M_{S_e} & M_{S_e} - M'_{F_t} \end{pmatrix}. \end{aligned} \tag{B2}$$

APPENDIX C: GREEN PART OF Ψ

Here we give the formula for the scalar product, which is needed to calculate the green part of the wave function Ψ as

$$\mathrm{gp} = \sum_{M_J=-3/2}^{3/2} \left\langle \Psi \middle| \frac{3}{2}, M_J \right\rangle \left\langle \frac{3}{2}, M_J \middle| \Psi \right\rangle. \tag{C1}$$

We find

$$\begin{aligned}\left\langle \Psi \middle| \frac{3}{2}, M_J \right\rangle \left\langle \frac{3}{2}, M_J \middle| \Psi \right\rangle = {} & \sum_{j=-1}^{1} \sum_{NLFF_tM_{F_t}} \sum_{F'F'_tM'_{F_t}} \sum_{M_{S_e}M_L} \frac{(R_1)^j_{NL}}{N+L+j+1} c_{(N+j)LJF'F'_tM'_{F_t}} c_{NLJFF_tM_{F_t}} \\ & \times (-1)^{F+F'+M_{F_t}+M'_{F_t}-2J+2M_J-1} [(2F+1)(2F_t+1)(2F'+1)(2F'_t+1)]^{\frac{1}{2}} \\ & \times \begin{pmatrix} F & \frac{1}{2} & F_t \\ M_L+M_J & M_{S_e} & -M_{F_t} \end{pmatrix} \begin{pmatrix} L & J & F \\ M_L & M_J & -M_L-M_J \end{pmatrix} \begin{pmatrix} F' & \frac{1}{2} & F'_t \\ M_L+M_J & M_{S_e} & -M'_{F_t} \end{pmatrix} \\ & \times \begin{pmatrix} L & J & F' \\ M_L & M_J & -M_L-M_J \end{pmatrix}. \end{aligned} \tag{C2}$$

The function $(R_1)^j_{NL}$ is taken from the recursion relations of the Coulomb-Sturmian functions in the Appendix of Ref. [10].

APPENDIX D: MATRIX ELEMENTS

In this section, we give the matrix elements of the terms in Eq. (25) in the basis of Eq. (28b) in Hartree units. The normalization factor $N^{(\alpha)}_{NL}$ is given in Eq. (27). All other matrix elements, which enter the symmetric matrices $\boldsymbol{D}$ and $\boldsymbol{M}$ in Eq. (29) and which are not given here, are listed in the Appendix of Ref. [10].

$$\begin{aligned}\langle \Pi' | \delta(\boldsymbol{r}) | \Pi \rangle = {} & \delta_{L'0}\delta_{L0}\delta_{JJ'}\delta_{F_tF'_t}\delta_{M_{F_t}M'_{F_t}} \frac{1}{\pi} (-1)^{F_t+F'+F+J+\frac{1}{2}} [(2F_t+1)(2F+1)(2F'+1)]^{\frac{1}{2}} \\ & \times \begin{Bmatrix} F' & F_t & \frac{1}{2} \\ F_t & F & 0 \end{Bmatrix} \begin{Bmatrix} 0 & F' & J \\ F & 0 & 0 \end{Bmatrix}, \end{aligned} \tag{D1}$$

$$\begin{aligned}\langle \Pi' | \boldsymbol{S}_e \cdot \boldsymbol{S}_h \, \delta(\boldsymbol{r}) | \Pi \rangle = {} & \delta_{L'0}\delta_{L0}\delta_{F_iF'_t}\delta_{M_{F_t}M'_{F_t}} \frac{3}{2\pi} (-1)^{F_t+F'+F+J+J'} [(2F+1)(2F'+1)(2J+1)(2J'+1)]^{\frac{1}{2}} \\ & \times \begin{Bmatrix} F' & F & 1 \\ \frac{1}{2} & \frac{1}{2} & F_t \end{Bmatrix} \begin{Bmatrix} F & F' & 1 \\ J' & J & 0 \end{Bmatrix} \begin{Bmatrix} \frac{1}{2} & J' & 1 \\ J & \frac{1}{2} & 1 \end{Bmatrix}, \end{aligned} \tag{D2}$$

$$\begin{aligned}\langle \Pi' | \frac{1}{r} e^{-r/\rho} | \Pi \rangle = {} & \delta_{LL'}\delta_{JJ'}\delta_{F_tF'_t}\delta_{M_{F_t}M'_{F_t}} \frac{1}{4} N^{(1)}_{N'L} N^{(1)}_{NL} \sum_{k=0}^{N'} \sum_{j=0}^{N} (-1)^{k+j} \binom{N'+2L+1}{N'-k} \binom{N+2L+1}{N-j} \\ & \times \frac{(2L+k+j+1)!}{k!\,j!} \left(\frac{2\rho}{1+2\rho} \right)^{(2+2L+k+j)}. \end{aligned} \tag{D3}$$

[1] R. Knox, *Theory of Excitons*, Solid State Physics Supplement Vol. 5, edited by H. Ehrenreich, F. Seitz, and D. Turnbull (Academic, New York, 1963).

[2] T. Kazimierczuk, D. Fröhlich, S. Scheel, H. Stolz, and M. Bayer, Nature (London) **514**, 343 (2014).

[3] J. Thewes, J. Heckötter, T. Kazimierczuk, M. Aßmann, D. Fröhlich, M. Bayer, M. A. Semina, and M. M. Glazov, Phys. Rev. Lett. **115**, 027402 (2015), and Supplementary Material.

[4] M. Aßmann, J. Thewes, D. Fröhlich, and M. Bayer, Nat. Mater. **15**, 741 (2016).

[5] F. Schweiner, J. Main, and G. Wunner, Phys. Rev. Lett. **118**, 046401 (2017).

[6] F. Schweiner, J. Main, and G. Wunner, Phys. Rev. B **93**, 085203 (2016).

[7] P. Grünwald, M. Aßmann, J. Heckötter, D. Fröhlich, M. Bayer, H. Stolz, and S. Scheel, Phys. Rev. Lett. **117**, 133003 (2016).

[8] M. Feldmaier, J. Main, F. Schweiner, H. Cartarius, and G. Wunner, J. Phys. B: At. Mol. Opt. Phys. **49**, 144002 (2016).

[9] F. Schöne, S.-O. Krüger, P. Grünwald, H. Stolz, S. Scheel, M. Aßmann, J. Heckötter, J. Thewes, D. Fröhlich, and M. Bayer, Phys. Rev. B **93**, 075203 (2016).

[10] F. Schweiner, J. Main, M. Feldmaier, G. Wunner, and Ch. Uihlein, Phys. Rev. B **93**, 195203 (2016).

[11] J. Heckötter, M. Freitag, D. Fröhlich, M. Aßmann, M. Bayer, M. A. Semina, and M. M. Glazov, Phys. Rev. B **95**, 035210 (2017).

[12] S. Zielińska-Raczyńska, D. Ziemkiewicz, and G. Czajkowski, Phys. Rev. B **95**, 075204 (2017).

[13] F. Schweiner, J. Main, G. Wunner, and Ch. Uihlein, Phys. Rev. B **94**, 115201 (2016).
[14] F. Schweiner, J. Main, G. Wunner, M. Freitag, J. Heckötter, Ch. Uihlein, M. Aßmann, D. Fröhlich, and M. Bayer, Phys. Rev. B **95**, 035202 (2017).
[15] S. Zielińska-Raczyńska, G. Czajkowski, and D. Ziemkiewicz, Phys. Rev. B **93**, 075206 (2016).
[16] S. Zielińska-Raczyńska, D. Ziemkiewicz, and G. Czajkowski, Phys. Rev. B **94**, 045205 (2016).
[17] Ch. Uihlein, D. Fröhlich, and R. Kenklies, Phys. Rev. B **23**, 2731 (1981).
[18] J. Luttinger, Phys. Rev. **102**, 1030 (1956).
[19] P. Schmelcher and L. S. Cederbaum, Z. Phys. D **24**, 311 (1992).
[20] N. O. Lipari and M. Altarelli, Phys. Rev. B **15**, 4883 (1977).
[21] G. Dasbach, D. Fröhlich, H. Stolz, R. Klieber, D. Suter, and M. Bayer, Phys. Rev. Lett. **91**, 107401 (2003).
[22] G. Dasbach, D. Fröhlich, H. Stolz, R. Klieber, D. Suter, and M. Bayer, Phys. Stat. Sol. (c) **2**, 886 (2005).
[23] G. Dasbach, D. Fröhlich, R. Klieber, D. Suter, M. Bayer, and H. Stolz, Phys. Rev. B **70**, 045206 (2004).
[24] L. Andreani, in *Strong Light-Matter Coupling: From Atoms to Solid-State Systems*, edited by A. Auffèves, D. Gerace, M. Richard, S. Portolan, M. Santos, L. Kwek, and C. Miniatura (World Scientific, Singapore, 2014), pp. 37–82.
[25] D. Fröhlich, R. Kenklies, Ch. Uihlein, and C. Schwab, Phys. Rev. Lett. **43**, 1260 (1979).
[26] G. M. Kavoulakis, Y.-C. Chang, and G. Baym, Phys. Rev. B **55**, 7593 (1997).
[27] A. Baldereschi and N. O. Lipari, Phys. Rev. B **3**, 439 (1971).
[28] A. Baldereschi and N. O. Lipari, Phys. Rev. B **9**, 1525 (1974).
[29] A. Baldereschi and N. O. Lipari, Phys. Rev. B **8**, 2697 (1973).
[30] M. Altarelli and N. O. Lipari, Phys. Rev. B **15**, 4898 (1977).
[31] K. Suzuki and J. C. Hensel, Phys. Rev. B **9**, 4184 (1974).
[32] G. Koster, J. Dimmock, R. Wheeler, and H. Statz, *Properties of the Thirty-Two Point Groups* (M.I.T. Press, Cambridge, MA, 1963).
[33] M. French, R. Schwartz, H. Stolz, and R. Redmer, J. Phys.: Condens. Matter **21**, 015502 (2009).
[34] *Polarons and Excitons in Polar Semiconductors and Ionic Crystals*, edited by J. Devreese and F. Peters, NATO ASI Series B, Vol. 108 (Plenum Press, New York, 1984).
[35] J. Dahl and A. Switzendick, J. Phys. Chem. Solids **27**, 931 (1966).
[36] R. Elliott, Phys. Rev. **124**, 340 (1961).
[37] L. Kleinman and K. Mednick, Phys. Rev. B **21**, 1549 (1980).
[38] H. Fröhlich, Adv. Phys. **3**, 325 (1954).
[39] Y. Toyozawa, J. Phys. Chem. Solids **25**, 59 (1964).
[40] J. Bardeen and W. Shockley, Phys. Rev. **80**, 72 (1950).
[41] H. Haken, Fortschr. Phys. **6**, 271 (1958).
[42] C. Klingshirn, *Semiconductor Optics*, 3rd ed. (Springer, Berlin, 2007).
[43] O. Madelung and U. Rössler, *Landolt-Börnstein*, New Series, Group III, Vol. 17 a to i, 22 a and b, 41 A to D (Springer, Berlin, 1982-2001).
[44] *Polarons and Excitons*, edited by C. Kuper and G. Whitefield (Oliver and Boyd, Edinburgh, 1963).
[45] H. Haken, Z. Phys. **146**, 527 (1956).
[46] H. Haken, Il Nuovo Cimento **3**, 1230 (1956).
[47] H. Haken, in *Halbleiterprobleme IV*, edited by W. Schottky (Vieweg, Berlin, 1957), pp. 1–48.
[48] H. Haken and W. Schottky, Z. Phys. Chem. **16**, 218 (1958).
[49] E. Menéndez-Proupin, C. L. B. Rios, and P. Wahnón, Phys. Status Solidi RRL **9**, 559 (2015).
[50] H.-R. Trebin, Phys. Stat. Sol (b) **92**, 601 (1979).
[51] U. Rössler and H.-R. Trebin, Phys. Rev. B **23**, 1961 (1981).
[52] H.-R. Trebin and U. Rössler, Phys. Stat. Sol. (b) **70**, 717 (1975).
[53] K. K. Bajaj, Solid State Commun. **15**, 1221 (1974).
[54] J. Pollmann and H. Büttner, Solid State Commun. **17**, 1171 (1975).
[55] S. Bednarek, J. Adamowski, and M. Suffczyński, Solid State Commun. **21**, 1 (1977).
[56] J. Pollmann and H. Büttner, Phys. Rev. B **16**, 4480 (1977).
[57] J. Hermanson, Phys. Rev. **150**, 660 (1966).
[58] K. Cho, Phys. Rev. B **14**, 4463 (1976).
[59] V. A. Kiselev and A. G. Zhilich, Sov. Phys. Solid State **13**, 2008 (1972).
[60] M. Denisov and V. Makarov, Phys. Stat. Sol. (b) **56**, 9 (1973).
[61] G. E. Pikus and G. L. Bir, Sov. Phys. JETP **33**, 108 (1971).
[62] P. D. Bloch and C. Schwab, Phys. Rev. Lett. **41**, 514 (1978).
[63] J. Heckötter, Stark-Effekt-Messungen an Rydberg Exzitonen in Cu_2O, Master's thesis, Technische Universität Dortmund, 2015.
[64] M. A. Caprio, P. Maris, and J. P. Vary, Phys. Rev. C **86**, 034312 (2012).
[65] A. Edmonds, *Angular Momentum in Quantum Mechanics* (Princeton University Press, Princeton, 1960).
[66] J. Broeckx, Phys. Rev. B **43**, 9643 (1991).
[67] E. Anderson, Z. Bai, C. Bischof, S. Blackford, J. Demmel, J. Dongarra, J. D. Croz, A. Greenbaum, S. Hammarling, A. McKenney, and D. Sorensen, LAPACK *Users' Guide*, 3rd ed. (Society for Industrial and Applied Mathematics, Philadelphia, PA, 1999).
[68] J. Hodby, T. Jenkins, C. Schwab, H. Tamura, and D. Trivich, J. Phys. C: Solid State Phys. **9**, 1429 (1976).
[69] H. E. Swanson and R. K. Fuyat, NBS Circular **539**, II:23 (1953).
[70] M. Inoue and Y. Toyozawa, J. Phys. Soc. Jpn. **20**, 363 (1965).
[71] T. R. Bader and A. Gold, Phys. Rev. **171**, 997 (1968).
[72] M. M. Denisov and V. P. Makarov, J. Phys. C **5**, 2651 (1972).
[73] V. T. A. an Yu. A. Stepanov, Sov. Phys. Solid State **17**, 1041 (1975).
[74] T. Gallagher, Rep. Prog. Phys. **51**, 143 (1988).
[75] A. Abragam and B. Bleaney, *Electron Paramagnetic Resonance of Transition Ions* (Clarendon Press, Oxford, 1970).